International Journal of Physical Sciences

Volume 8 Number 24 30 June, 2013
ISSN 1992-1950

Academic Journals

ABOUT IJPS

The **International Journal of Physical Sciences (IJPS)** is published weekly (one volume per year) by Academic Journals.

International Journal of Physical Sciences (IJPS) is an open access journal that publishes high-quality solicited and unsolicited articles, in English, in all Physics and chemistry including artificial intelligence, neural processing, nuclear and particle physics, geophysics, physics in medicine and biology, plasma physics, semiconductor science and technology, wireless and optical communications, materials science, energy and fuels, environmental science and technology, combinatorial chemistry, natural products, molecular therapeutics, geochemistry, cement and concrete research, metallurgy, crystallography and computer-aided materials design. All articles published in IJPS are peer-reviewed.

Submission of Manuscript

Submit manuscripts as e-mail attachment to the Editorial Office at: ijps@academicjournals.org. A manuscript number will be mailed to the corresponding author shortly after submission.

For all other correspondence that cannot be sent by e-mail, please contact the editorial office (at ijps@academicjournals.org).

The International Journal of Physical Sciences will only accept manuscripts submitted as e-mail attachments.

Please read the **Instructions for Authors** before submitting your manuscript. The manuscript files should be given the last name of the first author.

Editors

Editorial Board

Instructions for Author

Electronic submission of manuscripts is strongly encouraged, provided that the text, tables, and figures are included in a single Microsoft Word file (preferably in Arial font).

The **cover letter** should include the corresponding author's full address and telephone/fax numbers and should be in an e-mail message sent to the Editor, with the file, whose name should begin with the first author's surname, as an attachment.

Article Types

Three types of manuscripts may be submitted:

Regular articles: These should describe new and carefully confirmed findings, and experimental procedures should be given in sufficient detail for others to verify the work. The length of a full paper should be the minimum required to describe and interpret the work clearly.

Short Communications: A Short Communication is suitable for recording the results of complete small investigations or giving details of new models or hypotheses, innovative methods, techniques or apparatus. The style of main sections need not conform to that of full-length papers. Short communications are 2 to 4 printed pages (about 6 to 12 manuscript pages) in length.

Reviews: Submissions of reviews and perspectives covering topics of current interest are welcome and encouraged. Reviews should be concise and no longer than 4-6 printed pages (about 12 to 18 manuscript pages). Reviews are also peer-reviewed.

Review Process

All manuscripts are reviewed by an editor and members of the Editorial Board or qualified outside reviewers. Authors cannot nominate reviewers. Only reviewers randomly selected from our database with specialization in the subject area will be contacted to evaluate the manuscripts. The process will be blind review.

Decisions will be made as rapidly as possible, and the journal strives to return reviewers' comments to authors as fast as possible. The editorial board will re-review manuscripts that are accepted pending revision. It is the goal of the IJPS to publish manuscripts within weeks after submission.

Regular articles

All portions of the manuscript must be typed double-spaced and all pages numbered starting from the title page.

The Title should be a brief phrase describing the contents of the paper. The Title Page should include the authors' full names and affiliations, the name of the corresponding author along with phone, fax and E-mail information. Present addresses of authors should appear as a footnote.

The Abstract should be informative and completely self-explanatory, briefly present the topic, state the scope of the experiments, indicate significant data, and point out major findings and conclusions. The Abstract should be 100 to 200 words in length.. Complete sentences, active verbs, and the third person should be used, and the abstract should be written in the past tense. Standard nomenclature should be used and abbreviations should be avoided. No literature should be cited.

Following the abstract, about 3 to 10 key words that will provide indexing references should be listed.

A list of non-standard **Abbreviations** should be added. In general, non-standard abbreviations should be used only when the full term is very long and used often. Each abbreviation should be spelled out and introduced in parentheses the first time it is used in the text. Only recommended SI units should be used. Authors should use the solidus presentation (mg/ml). Standard abbreviations (such as ATP and DNA) need not be defined.

The Introduction should provide a clear statement of the problem, the relevant literature on the subject, and the proposed approach or solution. It should be understandable to colleagues from a broad range of scientific disciplines.

Materials and methods should be complete enough to allow experiments to be reproduced. However, only truly new procedures should be described in detail; previously published procedures should be cited, and important modifications of published procedures should be mentioned briefly. Capitalize trade names and include the manufacturer's name and address. Subheadings should be used. Methods in general use need not be described in detail.

Results should be presented with clarity and precision. The results should be written in the past tense when describing findings in the authors' experiments. Previously published findings should be written in the present tense. Results should be explained, but largely without referring to the literature. Discussion, speculation and detailed interpretation of data should not be included in the Results but should be put into the Discussion section.

The Discussion should interpret the findings in view of the results obtained in this and in past studies on this topic. State the conclusions in a few sentences at the end of the paper. The Results and Discussion sections can include subheadings, and when appropriate, both sections can be combined.

The Acknowledgments of people, grants, funds, etc should be brief.

Tables should be kept to a minimum and be designed to be as simple as possible. Tables are to be typed double-spaced throughout, including headings and footnotes. Each table should be on a separate page, numbered consecutively in Arabic numerals and supplied with a heading and a legend. Tables should be self-explanatory without reference to the text. The details of the methods used in the experiments should preferably be described in the legend instead of in the text. The same data should not be presented in both table and graph form or repeated in the text.

Figure legends should be typed in numerical order on a separate sheet. Graphics should be prepared using applications capable of generating high resolution GIF, TIFF, JPEG or Powerpoint before pasting in the Microsoft Word manuscript file. Tables should be prepared in Microsoft Word. Use Arabic numerals to designate figures and upper case letters for their parts (Figure 1). Begin each legend with a title and include sufficient description so that the figure is understandable without reading the text of the manuscript. Information given in legends should not be repeated in the text.

References: In the text, a reference identified by means of an author‘s name should be followed by the date of the reference in parentheses. When there are more than two authors, only the first author‘s name should be mentioned, followed by ’et al‘. In the event that an author cited has had two or more works published during the same year, the reference, both in the text and in the reference list, should be identified by a lower case letter like ’a‘ and ’b‘ after the date to distinguish the works.

Examples:

Abayomi (2000), Agindotan et al. (2003), (Kelebeni, 1983), (Usman and Smith, 1992), (Chege, 1998; 1987a,b; Tijani, 1993,1995), (Kumasi et al., 2001)

References should be listed at the end of the paper in alphabetical order. Articles in preparation or articles submitted for publication, unpublished observations, personal communications, etc. should not be included in the reference list but should only be mentioned in the article text (e.g., A. Kingori, University of Nairobi, Kenya, personal communication). Journal names are abbreviated according to Chemical Abstracts. Authors are fully responsible for the accuracy of the references.

Examples:

Ogunseitan OA (1998). Protein method for investigating mercuric reductase gene expression in aquatic environments. Appl. Environ. Microbiol. 64:695-702.

Gueye M, Ndoye I, Dianda M, Danso SKA, Dreyfus B (1997). Active N2 fixation in several Faidherbia albida provenances. Ar. Soil Res. Rehabil. 11:63-70.

Charnley AK (1992). Mechanisms of fungal pathogenesis in insects with particular reference to locusts. In: Lomer CJ, Prior C (eds) Biological Controls of Locusts and Grasshoppers: Proceedings of an international workshop held at Cotonou, Benin. Oxford: CAB International, pp 181-190.

Mundree SG, Farrant JM (2000). Some physiological and molecular insights into the mechanisms of desiccation tolerance in the resurrection plant Xerophyta viscasa Baker. In Cherry et al. (eds) Plant tolerance to abiotic stresses in Agriculture: Role of Genetic Engineering, Kluwer Academic Publishers, Netherlands, pp 201-222.

Short Communications

Short Communications are limited to a maximum of two figures and one table. They should present a complete study that is more limited in scope than is found in full-length papers. The items of manuscript preparation listed above apply to Short Communications with the following differences: (1) Abstracts are limited to 100 words; (2) instead of a separate Materials and Methods section, experimental procedures may be incorporated into Figure Legends and Table footnotes; (3) Results and Discussion should be combined into a single section.

Proofs and Reprints: Electronic proofs will be sent (e-mail attachment) to the corresponding author as a PDF file. Page proofs are considered to be the final version of the manuscript. With the exception of typographical or minor clerical errors, no changes will be made in the manuscript at the proof stage.

International Journal of Physical Sciences

Table of Contents: Volume 8 Number 24 30 June, 2013

ARTICLES

academicJournals

Vol. 8(24), pp. 1298-1306, 30 June, 2013
DOI: 10.5897/IJPS2013.3922
ISSN 1992 - 1950 © 2013 Academic Journals
http://www.academicjournals.org/IJPS

International Journal of Physical Sciences

Full Length Research Paper

Linearization of Zoeppritz equations and practical utilization

Oladapo, Michael Ilesanmi

Department of Applied Geophysics, Federal University of Technology, Akure, Nigeria.

Accepted 21 June, 2013

The theory and practical utilization of simplification of the original general expressions for the reflection of compression and shear waves at a boundary as a function of the densities and velocities of layers in contact are presented in this paper. The original general expressions are highly non-linear and presumed to defy physical insight. Elimination of the properties of V_s and ΔV_s in favour of σ and $\Delta\sigma$ enabled the success of a two-term approximation and revealed the surprising effects of Poisson's ratio on P-wave reflection coefficient which was a neglected elastic constant. The simplified equation was further expressed in terms of angular reflections to obtain first order reflectivity expression in terms of R_p and R_s. The number of unknown parameters is thus reduced by assuming that the fractional changes in material parameters are small across layer interfaces. Simplification of the equation has brought into existence the Amplitude Variation Offset (AVO) attributes with successful practical utilization in hydrocarbon delineation in many oil fields including the Niger Delta Slope. Determination of the terms of the linearized equation from rock properties and seismic events remains of vital value in practice as demonstrated in the evaluation of hydrocarbon potential in North-Built field.

Key words: Compressional and shear waves, densities, velocities, Poisson's ratio, amplitude variation offset (AVO) attributes, hydrocarbon.

INTRODUCTION

Knott (1899) and Zoeppritz (1919) deduced the general expressions for the reflection of compression and shear waves at a boundary as a function of the densities and velocities of layers in contact. The unwieldy nature of the equations makes visualising how the variation of a particular parameter will affect the reflection coefficient curve very difficult (Castagna, 1993). Realising that the simplifications and approximations of the equations are desirable in order to apply them, Aki and Richards (1980) gave a more convenient form. This work is thus aimed at the practical utilization of the Zoeppritz equations approximations in North-Built field of the Niger Delta Slope.

The Zoeppritz's equations satisfying four boundary conditions are in the following forms (Sheriff and Geldart 1982):

$$A_1\cos\theta_1 - B_1\sin\phi_1 + A_2\cos\theta_2 + B_2\sin\phi_2 = A_0\cos\theta_1 \quad (1)$$

$$A_1\sin\theta_1 + B_1\cos\phi_1 - A_2\sin\theta_2 + B_2\cos\phi_2 = A_0\sin\theta_1 \quad (2)$$

$$A_1Z_1\cos 2\phi_1 - B_1\omega_1\sin 2\phi_1 - A_2Z_2\cos 2\phi_1 - B_2\omega_2\sin 2\phi_2 = -A_0Z_1\cos 2\phi_1 \quad (3)$$

$$A_1\gamma_1\omega_1\sin 2\theta_1 + B_1\omega_1\cos 2\phi_1 + A_2\gamma_2\omega_2\sin\theta_2 - B_2\omega_2\cos 2\phi_2 = A_0\gamma_1\omega_1\sin 2\theta_1 \quad (4)$$

Where $Z_i = \rho_i V_{pi}$; $\omega_i = \rho_i V_{si}$ (5)

E-mail: oladapom@yahoo.co.uk.

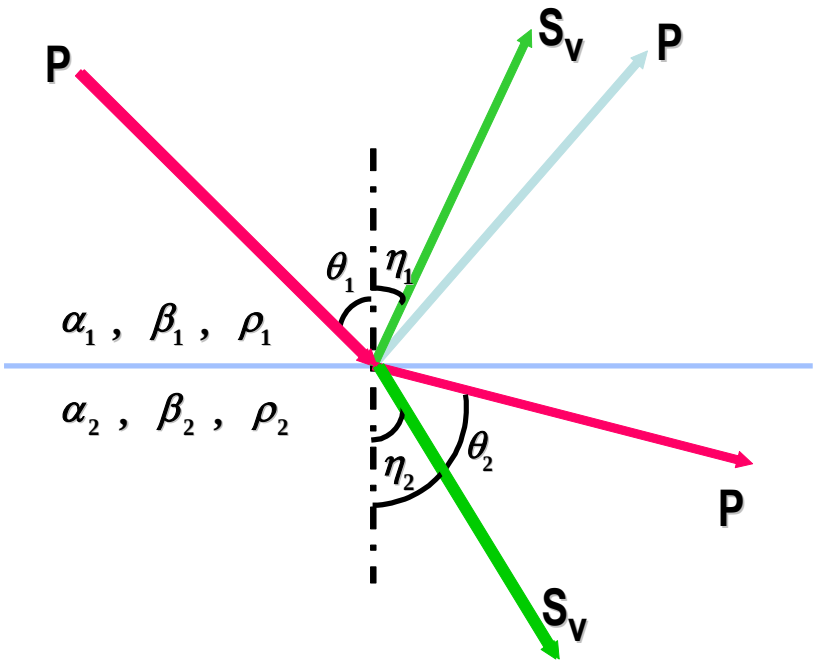

Figure 1. Stresses and displacement across the boundary of elastic media.

$$\gamma_i = \frac{\omega_i}{Z_i} = \frac{V_{si}}{V_{pi}} \qquad \text{i = 1, 2.....n} \qquad (6)$$

These equations yield amplitudes that are accurate up to the critical angle as their description does not include head-wave energy (Sheriff, 2002). The equations assume continuity of stress and displacement at the interface.

At an interface, the densities and velocities in each of the media must be known, and then $Z_1, Z_2, \omega_1, \omega_2, \gamma_1$ and γ_2 can be derived. If A_0 and θ_1 are known, then θ_2, λ_2 and λ_1 can be computed to obtain amplitudes A_1, A_2, B_1, and B_2.

For a normal incident P-wave, $\theta_1, \theta_2, \lambda_1$ and λ_2 reduce to zero hence $\cos\theta_1 = \cos\theta_2 = 1$, then $\sin\theta_1 = \sin\theta_2 = 0$.

In practice, detectors only respond to the longitudinal component of the waves, therefore, B_1 and B_2 do not exist. Thus:

$$A_1 + A_2 = A_0 \qquad (7)$$

That is $$T = \frac{2\rho_1 V_1}{\rho_1 V_1 + \rho_2 V_2} \qquad (8)$$

T is the transmission coefficient.

Therefore, $$R = \frac{A_1}{A_0} = \frac{\rho_2 V_2 - \rho_1 V_1}{\rho_2 V_2 + \rho_1 V_1} \qquad (9)$$

If the incident wave intercepts the interface obliquely, the situation becomes more complicated because the *R* is a tortuous function of the angle of incidence; the densities of the two bounding media; the ratio of velocities of the two media and the Poisson's ratio contrast of the two media (Figure 1).

Aki and Richards (1980) and Waters (1981) gave the equations in matrix form as:

$$\begin{bmatrix} \sin\theta & \cos\phi & -\sin\theta` & \cos\phi` \\ -\cos\theta & \sin\phi & -\cos\theta` & -\sin\phi` \\ \sin 2\theta & \frac{V_{p1}}{V_{s1}}\cos 2\phi & \frac{\rho_2 V_{s2}^2 V_{p1}}{\rho_1 V_{s1}^2 V_{p2}}\sin 2\theta` & -\frac{\rho_2 V_{s2} V_{p1}}{\rho_1 V_{s1}^2}\cos 2\phi` \\ \cos 2\theta & \frac{V_{s1}}{V_{p1}}\sin 2\phi & -\frac{\rho_2 V_{p2}}{\rho_1 V_{p1}^2}\cos 2\phi` & -\frac{\rho_2 V_{s2}}{\rho_1 V_{P1}^2}\sin 2\phi` \end{bmatrix} \begin{bmatrix} R_P \\ R_S \\ T_P \\ T \end{bmatrix} = \begin{bmatrix} -\sin\theta \\ -\cos\phi \\ \sin 2\theta \\ -\cos 2\phi \end{bmatrix} \qquad (10)$$

APPROXIMATION OF ZOEPPRITZ'S EQUATIONS

The Zoeppritz's equations are highly non-linear with respect to velocities and densities (Spratt et al., 1993). From the matrix description of the Zoeppritz equations, Aki and Richards (1980) derived the following formula:

$$R(\theta) \approx \frac{1}{2}\left(1 - 4\left(\frac{V_S}{V_P}\right)^2 \sin^2\theta\right)\frac{\Delta\rho}{\rho} + \frac{\sec^2\theta}{2}\frac{\Delta V_P}{V_P} - \left(\frac{4V_S}{V_P}\right)^2 \sin^2\theta \frac{\Delta V_S}{V_S} . \qquad (11)$$

Where the elastic properties are related as follows to those on each side of the interface

$$\Delta V_P = (V_{P2} - V_{P1}) \quad and \quad V_P = (V_{P2} + V_{P1})/2 \tag{12}$$

$$\Delta V_S = (V_{S2} - V_{S1}) \quad and \quad V_S = (V_{S2} + V_{S1})/2 \tag{13}$$

$$\Delta\rho = (\rho_2 - \rho_1) \quad and \quad \rho = (\rho_2 + \rho_1)/2 \tag{14}$$

The angle □ is the average of incidence and transmission angles $\theta = (\theta_2 + \theta_1)/2$.

By proposing a polynomial fit for the reflectivity that is accurate for an angle of incidence up to 35°, Shuey (1985) modified Equation (11) by eliminating the properties V_S, ΔV_S in favour of σ, Δσ

$$\Delta\sigma = (\sigma_2 - \sigma_1) \quad and \quad \sigma = (\sigma_2 + \sigma_1)/2 \tag{15}$$

The substitution is effected using the equation

$$V_S^{\,2} = V_P^{\,2}\,\frac{1-2\sigma}{2(1-\sigma)} \tag{16}$$

R_0 and the amplitude at NI were factored out by the differential of Equation (11) thus resulting in

$$R(\theta)/R_0 \approx 1 + A\sin^2\theta + B(\tan^2\theta - \sin^2\theta) \tag{17}$$

Where,

$$R_0 = \frac{1}{2}\left(\frac{\Delta V_P}{V_P} + \frac{\Delta\rho}{\rho}\right) \tag{18}$$

$$A = A_0 + \frac{1}{(1-\sigma)^2}\frac{\Delta\sigma}{R_0} \tag{19}$$

$$A_0 = B - 2(1+B)\frac{1-2\sigma}{1-\sigma} \tag{20}$$

and

$$B = \frac{\Delta V_P/V_P}{\Delta V_P/V_P + \Delta\rho/\rho} \tag{21}$$

Multiplying Equation (17) through by R_0

$$R(\theta) \approx R_0 + \left[A_0 R_0 + \frac{\Delta\sigma}{(1-\sigma)^2}\right]\sin^2\theta + \frac{1}{2}\frac{\Delta V_P}{V_P}(\tan^2\theta - \sin^2\theta) \tag{22}$$

Equation (22) displays, which combinations of elastic properties are effective in successive ranges of angle θ. The first term gives the amplitude at normal incidence $(\theta = 0)$, the second term characterises *R (θ)* at intermediate angles, and the third term describes the approach to critical angle.

Castagna et al. (1998) adopted Swan, (1993) approach to express the Aki and Richards (1980) (Equation 12) for the Richards and Frasier (1976) approximation in terms of the angular reflections A, B and C:

$$R(\theta) \approx A + B\sin^2(\theta) + C\sin^2(\theta)\tan^2(\theta) \tag{23}$$

where

$$A = \frac{1}{2}\left(\frac{\Delta V_P}{V_P} + \frac{\Delta\rho}{\rho}\right); \tag{24}$$

$$B = \frac{1}{2}\frac{\Delta V_P}{V_P} - 2\left(\frac{V_S}{V_P}\right)^2\left(2\frac{\Delta V_S}{V_S} + \frac{\Delta\rho}{\rho}\right); \tag{25}$$

$$C = \frac{1}{2}\frac{\Delta V_P}{V_P} \tag{26}$$

Spratt et al. (1993) derived the first order reflectivity expressions from Equation (11) (in order to reduce the number of parameters that can be uniquely found) by assuming that the fractional changes in material parameters are small across the interface.

Assuming the incident angle is small while only terms to first order in $\sin^2\theta$ are retained, Equation (13) becomes:

$$R(\theta) = \frac{1}{2}\left[1 - 4\left(\frac{V_S}{V_P}\right)^2\sin^2\theta\right]\frac{\Delta\rho}{\rho} + \frac{1}{2}(1+\sin^2\theta)\frac{\Delta V_P}{V_P} - 4\left(\frac{V_S}{V_P}\right)^2\frac{\Delta V_S}{V_S}\sin^2\theta \tag{27}$$

Rearranging the terms gives:

$$R(\theta) = \frac{1}{2}\left(\frac{\Delta\rho}{\rho} + \frac{\Delta V_P}{V_P}\right) + \left[\frac{1}{2}\left(\frac{\Delta\rho}{\rho} + \frac{\Delta V_P}{V_P}\right) - 8\left(\frac{V_S}{V_P}\right)^2\frac{1}{2}\left(\frac{\Delta\rho}{\rho} + \frac{\Delta V_P}{V_P}\right)\right]\sin^2\theta + \left[2\left(\frac{V_S}{V_P}\right)^2 - \frac{1}{2}\right]\frac{\Delta\rho}{\rho}\sin^2\theta$$

or

$$R(\theta) = R_P + (R_P - 2*R_S)\sin^2\theta + 0*\frac{\Delta\rho}{\rho}\sin^2\theta \tag{28}$$

where

$$R_P = \frac{1}{2}\left(\frac{\Delta\rho}{\rho} + \frac{\Delta V_P}{V_P}\right),\ R_S = \frac{1}{2}\left(\frac{\Delta\rho}{\rho} + \frac{\Delta V_S}{V_S}\right),\ \ 2* = 8\left(\frac{V_S}{V_P}\right)^2,\ \ 0* = 2\left(\frac{V_S}{V_P}\right)^2 - \frac{1}{2}.$$

$R_P\ and\ R_S$ are the compression and shear reflectivity respectively (correct to first order in the Δ's).

If $\frac{V_P}{V_S}$ = 2, then 2* = 2 and 0* = 0 and the expression reduces to

$$R(\theta) \approx R_P + (R_P - 2R_S)\sin^2\theta \quad (29)$$

In most sedimentary basins, small changes in density can be expressed as small changes in (compressional) velocity, (Ross, 2000) such that

$$\frac{\Delta\rho}{\rho} \approx \frac{g\Delta V_P}{V_P} \quad (30)$$

Where $g = 0.25\left[2\left(\frac{V_s}{V_p}\right) - \frac{1}{2}\right]$ is an expansion coefficient for other effects in higher-order corrections. Using Equation (30), (24) and (25) can be rewritten as Equations (31) and (32) respectively assuming $\frac{V_p}{V_s}$ remains constant;

$$A = \frac{5}{8}\frac{\Delta V_P}{V_P} \quad (31)$$

$$B = \frac{4}{5}A - 2\gamma^2\left(2\frac{\Delta V_S}{V_S} + \frac{2}{5}A\right) \quad (32)$$

By substituting equation (31) into equation (32) and letting $\frac{V_S}{V_P}$ = γ,

$$B = \frac{1}{2}\frac{\Delta V_P}{V_P} - 2\left[\frac{V_S}{V_P}\right]^2\left(2\frac{\Delta V_S}{V_S} + \frac{1}{4}\frac{\Delta V_P}{V_P}\right) \quad (33)$$

which can be further reduced to

$$B = \frac{4}{5}A(1-\gamma)^2 - 4\gamma^2\frac{\Delta V_s}{V_s} \quad (34)$$

The simplification of the P-wave reflection coefficient given by Zoeppritz to various expressions (Equations 12 to 34) has enabled the determination and application of what is popularly referred to as Amplitude Variation with Offset (AVO) attributes. The three most commonly used approximations are:

$$R(\theta) \approx A + B\sin^2(\theta) \quad (35)$$

$$R(\theta) \approx R_p\left(1 + \tan^2\theta\right) - 2R_s\sin^2\theta \quad (36)$$

$$R(\theta) \approx NI\cos^2\theta + PR\sin^2\theta \quad (37)$$

Where, R = reflection coefficient; θ = angle of incidence; A = AVO intercept; B = AVO gradient.

Equation (35) is the original two-term Shuey (1985) equation, where the higher terms have been dropped by limiting the angle of incidence to $\theta < 30°$. Equation (36) was introduced by Fatti et al. (1994) while Verm and Hilterman (1995) introduced Equation (37). A is the normal incidence (NI) attribute while B is the Poisson Reflectivity (PR) attribute.

Within the range of incidence angles (up to 35°) typically used in exploration (Seriff et al., 1980), Equations (35) to (37) can be considered equivalent, hence we have:

$$A = NI = R_p \quad (38a)$$

$$B = R_p - 2R_s \quad (38b)$$

$$R_s = \frac{A-B}{2} \quad \text{Pseudoshear} \quad (38c)$$

$$PR = 2(R_p - R_s) = A + B \quad (38d)$$

R_s is normal incidence S-wave reflection coefficient which is called pseudo shear because it is strictly the shear only when V_p/V_s = 2 (Hendrickson et al. 1991). From the approximations of Zoeppritz's equations, determination of A and B values of the linearized version of the equation becomes imperative. This can be obtained from rock property measurements in well logs (Oladapo and Adetola, 2005) and seismic events (Figure 2).

PRACTICAL UTILIZATION

Ostrander (1984) in the first practical approach to AVO, proposed a method that could distinguish between gas-related amplitude anomalies and non-gas-related anomalies. The change in zero-offset reflectivity R_0, or intercept, is the most diagnostic feature. The seismic response depends on the encasing geology, porefill, and interference effects (Veeken and Rauch-Davies, 2006). AVO interpretation may be enhanced by cross plotting

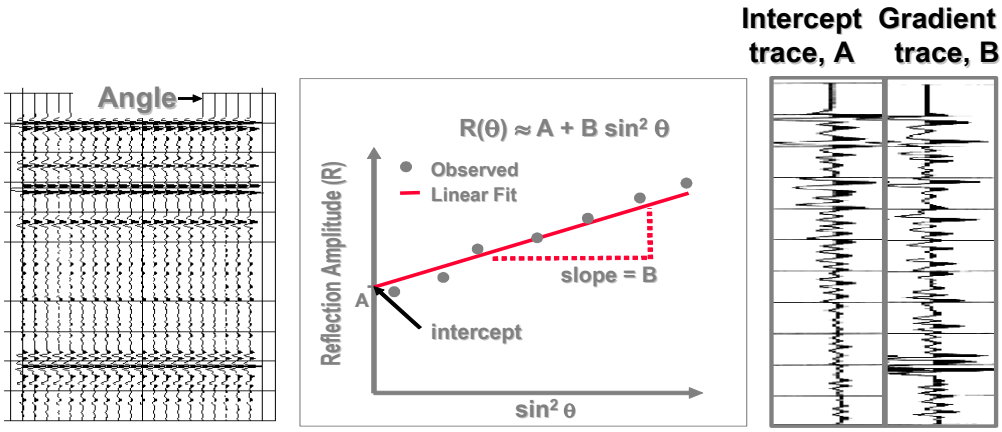

Figure 2. AVO Gradient and intercept.

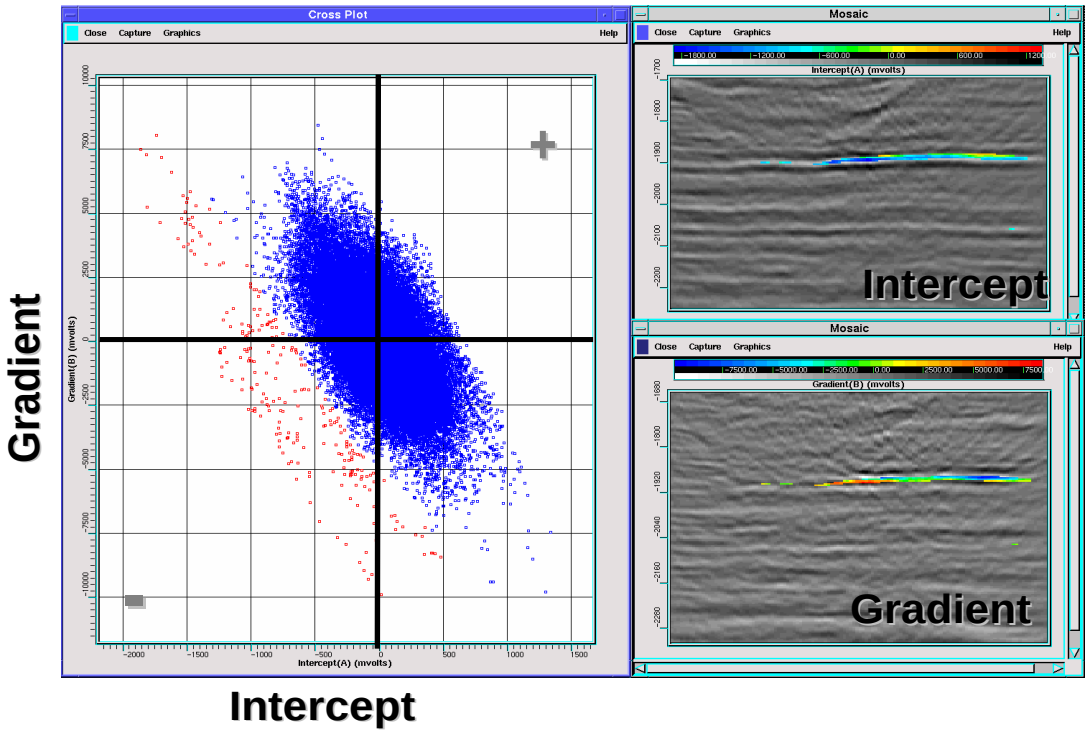

Figure 3. AVO Crossplot from a Niger Delta slope prospect. The highlighted points (red) on the crossplot indicate points that are anomalous due to fluid effects.

the AVO NI (Normal Incidence) intercept (A) and gradient RP (Poisson Reflectivity) (B) two parameters obtained from Shuey's two-term approximation of Zoeppritz's equations (Smith and Gidlow, 1987; Foster et al., 1993; Ross, 2000; Veeken et al., 2002; Oladapo et al., 2009; Kim et al., 2011; Hossain et al., 2012). Under a variety of reasonable petrophysical assumptions, brine-saturated sandstones and shale follow a well-defined "background" trend in an Intercept-Gradient plane. Hilterman (1987) observed that A and B are generally negatively correlated for background rocks. Deviations from the background trend may be indicative of hydrocarbons or lithology with anomalous properties. Typical attributes crossplot from Niger Delta Slope field is presented in Figure 3.

In the Niger Delta, AVO analyses have been successfully utilized for the detection and mapping of gas (Osuntola et al., 1997; Oladapo et al., 2009). A semi quantitative AVO analysis of a horizon (termed BB within

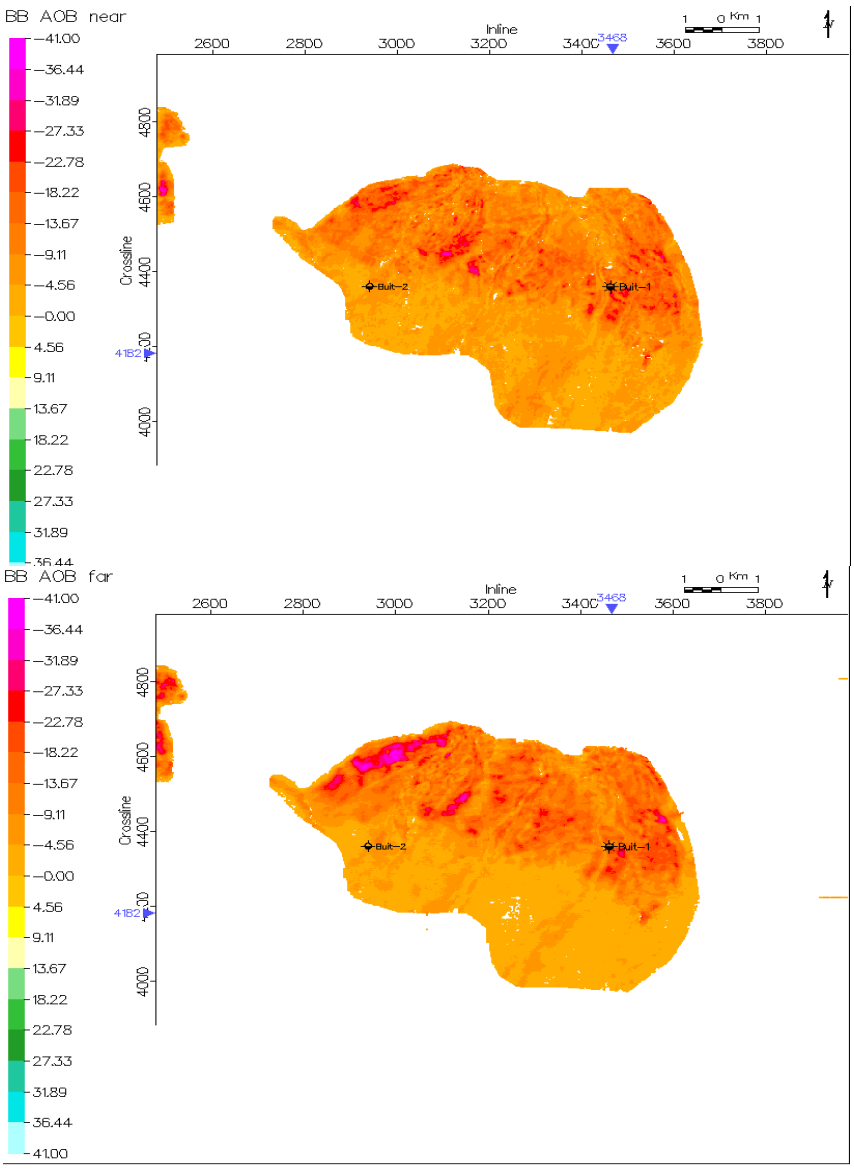

Figure 4. Sub-Stacks Amplitude maps of Buit-BB horizon.

time window of 2.668 s) within Buit North field of Niger Delta Slope was evaluated using the two parameter AVO attributes. Applications of Intercept and Gradient for Buit-North Field Evaluation are:

Near amplitude $a_n = A + B\sin^2\theta_n$ (39)

Far amplitude $a_f = A + B\sin^2\theta_f$ (40)

Solving this for B and for A for near and far stack:

$$a_f - a_n = B\left(\sin^2\theta_f - \sin^2\theta_n\right)$$

$$B = \frac{\left(a_f - a_n\right)}{\left(\sin^2\theta_f - \sin^2\theta_n\right)} \quad (41)$$

$$A = \frac{a_f \sin^2\theta_n - a_n \sin^2\theta_f}{\sin^2\theta_n - \sin^2\theta_f} \quad (42)$$

Pairs of far and full, and the near and far offset data (using Equations 39 and 40) were utilised for generating BB horizon substacks maps (Figure 4). The average angles used for the sub-stacks are near 10°, far 22.5°, full 27.5°. Using Amplitude/Background normal (a/b or AOB) approach, Equations 39 and 40 becomes:

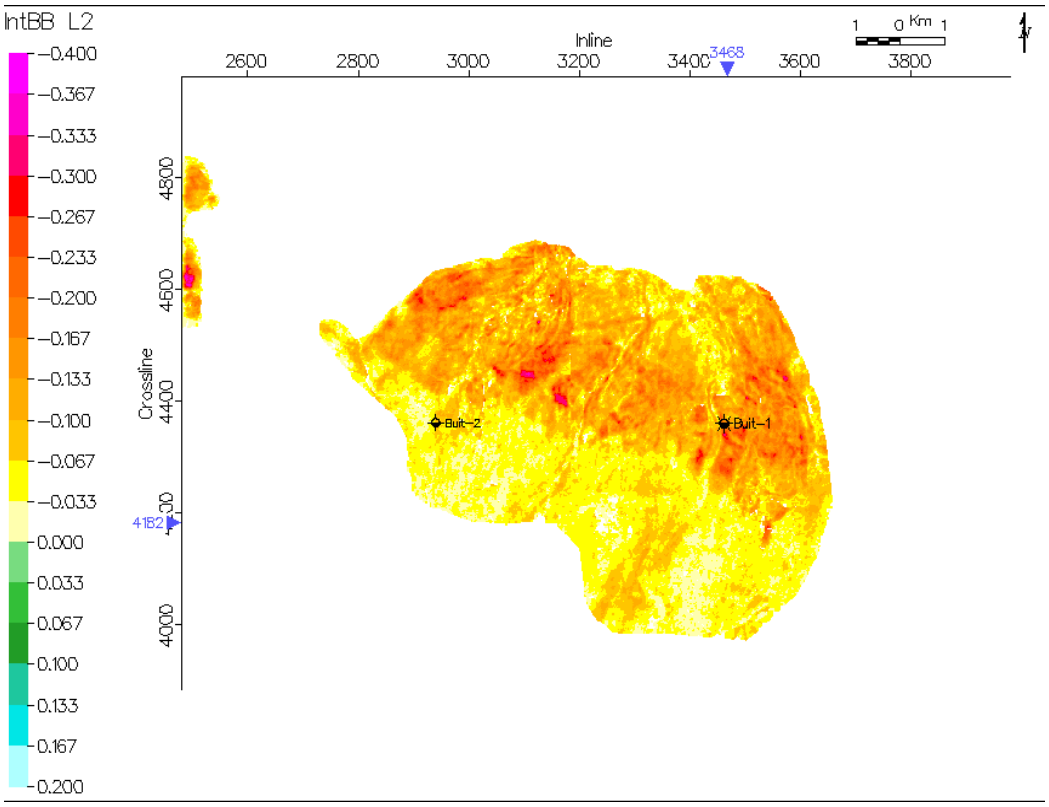

Figure 5. Intercept (A) amplitude map of Buit-BB horizon.

$$a/b_{near} = A + B\sin^2\theta_{near} \quad (43)$$

$$a/b_{far} = A + B\sin^2\theta_{far} \quad (44)$$

$$B = \frac{\left(a/b_{far} - a/b_{near}\right)}{\left(\sin^2\theta_{far} - \sin^2\theta_{near}\right)} \quad (45)$$

$$A = \frac{a/b_{far}\sin^2\theta_{near} - a/b_{near}\sin^2\theta_{far}}{\sin^2\theta_{near} - \sin^2\theta_{far}} \quad (46).$$

Similar computations were undertaken for the full and far data. The average of the two results utilised for generating Intercept and Gradient maps (designated L and M respectively) shown in Figures 5 and 6 are as follows:

$$B = \frac{a/b_{near}}{2\left(\sin^2\theta_{near} - \sin^2\theta_{far}\right)} + \frac{a/b_{full}}{2\left(\sin^2\theta_{full} - \sin^2\theta_{far}\right)} - a/b_{far}\frac{\left[\left(\sin^2\theta_{full} - \sin^2\theta_{far}\right) + \left(\sin^2\theta_{near} - \sin^2\theta_{far}\right)\right]}{\left[\left(\sin^2\theta_{full} - \sin^2\theta_{far}\right)\left(\sin^2\theta_{near} - \sin^2\theta_{far}\right)\right]} \quad (47)$$

$$A = a/b_{far}\left[1 + \left(\frac{\sin^2\theta_{far}}{2\left(\sin^2\theta_{near} - \sin^2\theta_{far}\right)}\right) + \left(\frac{\sin^2\theta_{far}}{2\left(\sin^2\theta_{full} - \sin^2\theta_{far}\right)}\right)\right] - a/b_{near}\left(\frac{\sin^2\theta_{far}}{2\left(\sin^2\theta_{near} - \sin^2\theta_{far}\right)}\right) - A/B_{full}\left(\frac{\sin^2\theta_{far}}{2\left(\sin^2\theta_{full} - \sin^2\theta_{far}\right)}\right) \quad (48)$$

The above equations exhibit the dependence of intercept and gradient on a/b (AOB) values of near, far and full stack. The computation is analogous to regression with four points, once for near and full and twice for far stack. The horizon is characterised by higher amplitudes on both the intercept and gradient sections that are diagnostic of class III gas sand using the classifications of Rutherford and Williams (1989). The seismic attribute A (or L), B (or M) and Background normal (Bn) maps (Figures 4, 5, 6 and 7) show rising AVO profiles within the horizon.

Conclusion

These semi-quantitative AVO tools are effective hydrocarbon indicators (HCI) as displayed within BB horizon. Hydrocarbon potential rating (which is apparently higher at the north-western flank of the field) can be achieved using the approximation attributes. This

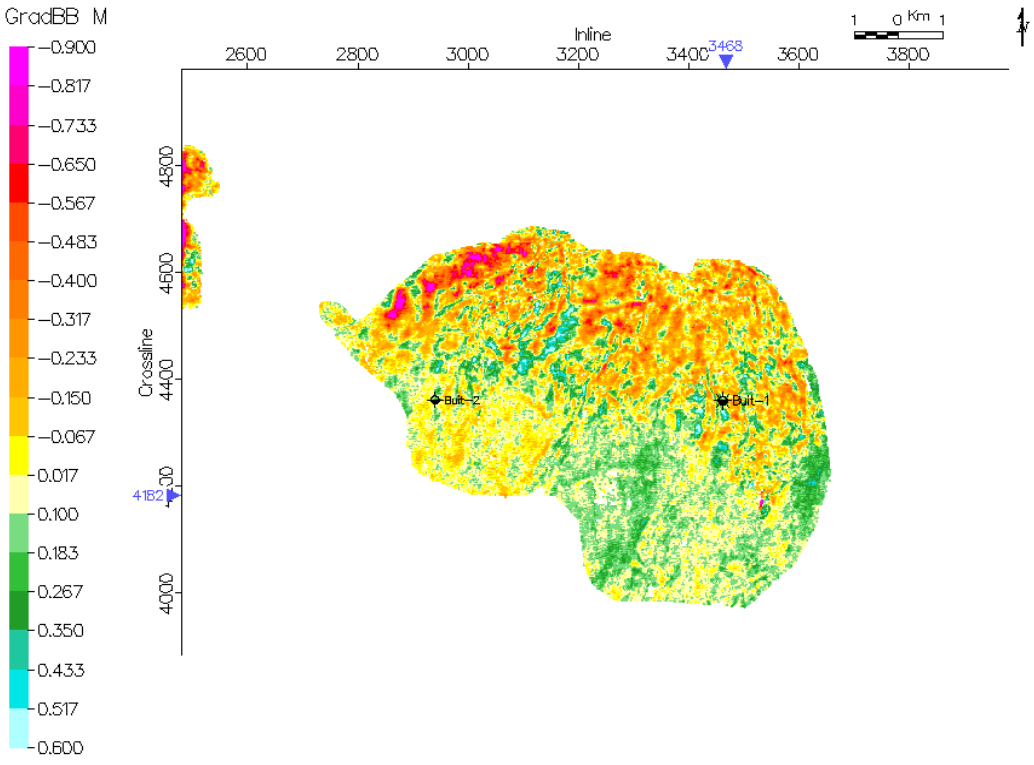

Figure 6. Gradient (B) map of Buit-BB horizon.

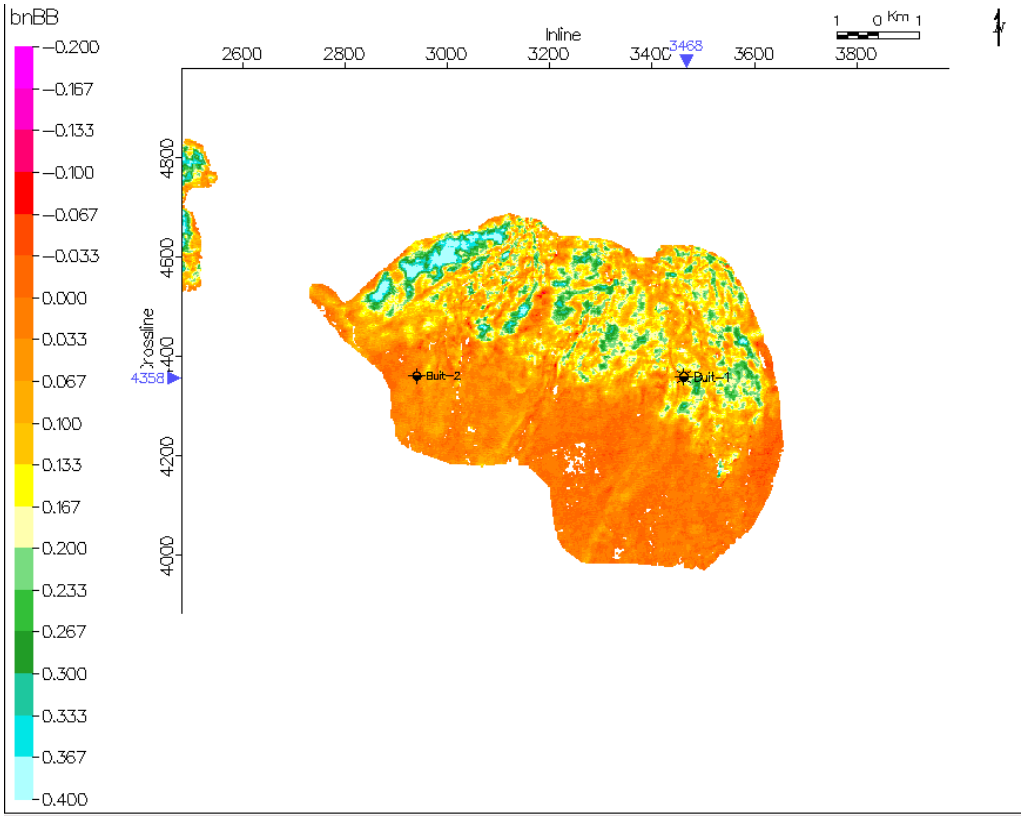

Figure 7. Background normal (bn) map of Buit-BB horizon.

assumption is based on the consistently higher AVO profile (AVO gradient and normal incidence amplitude) characterising the north-western section of the horizon.

REFERENCES

Aki K, Richards PG (1980). Quantitative Seismology: Theory and Methods. W.H. Freeman and Co.

Castagna JP (1993). Petrophysical imaging using AVO. The Leading Edge, 12(3):172-178.

Castagna JP, Swan HW, Foster JD (1998). Framework for AVO gradient and intercept interpretation: Geophysics 63:948–956.

Fatti JL, Smith GC, Vail PJ, Levitt PR (1994). Detection of gas in sandstone reservoirs using AVO analysis: A 3-D seismic case history using the Geostack technique. Geophysics 59:362-1376.

Hendrickson JS, Li SM, Daste AS, Gunther GL (1991). Evidence for AVO as a direct hydrocarbon indicator and a direct no-hydrocarbon indicator. Shell Geophysical conference paper No. 100.

Hossain Z, Mukerji T, Fabricius IL (2012). Vp-Vs relationship and amplitude variation with offset modelling of glauconitic greensand‡. Geophysical Prospecting, 60:117–137. doi: 10.1111/j.1365-2478.2011.00968.x

Kim JS, Won-Ki K, Hee-Sang H, Sung-Soo K (2011). AVO analysis using crossplot and amplitude polynomial methods for characterisation of hydrocarbon reservoirs Exploration Geophysics 42(1):25-41 http://dx.doi.org/10.1071/EG10048

Knott CG (1899). Reflection and refraction of elastic waves, with seismological applications. Phil. Mag., 5th ser. 48:64–97.

Oladapo MI, Adetola BA (2005). Rock property trend analyses in the Niger Delta Slope. Nanjing Institute of Geophysical Prospecting and Institute of Physics Publishing. J. Geophys. Eng. 2:103–110.

Oladapo MI, Ojo JS Olorunfemi MO, Adetola BA (2009). Monte-Carlo Modeling of Some Niger Delta Slope Events. J. Appl. Sci. 9(5):883-891.

Ostrander WJ (1984). Plane-wave reflection coefficients for gas-sands at non-normal angles of incidence: Geophysics 49:1637- 1648.

Osuntola OK, Ojo JS, Maxwell BA (1997). Interpreting the Amplitude Versus Offset (AVO) analysis results. Paper presented at the 15th Annual Conference of the Nigerian Association of Petroleum Explorationists.

Richards PG, Frasier CW (1976). Scattering of elastic wave from depth-dependent inhomogeneities: Geophysics, 41:441 – 458.

Ross CP (2000). Effective AVO crossplot modelling: A tutorial. Geophysics 65:700-711.

Rutherford SR, Williams RH (1989). Amplitude-versus Offset variations in gas sands: Geophysics, 54:680–688.

Seriff AJ, Thayer RE, Sriram KP, Cooper MR (1980). Vp and Vs of sedimentary rocks, Items 230-13102.00, Monthly Research Summary, Shell Development Bellaire Research Center, Houston, November.

Sheriff RE, Geldart LP (1982). Exploration Seismology. Volume 1, Cambridge University Press.

Sheriff RE (2002). Encyclopedic Dictionary of Exploration Geophysics, 4th edn. SEG, Tulsa.

Shuey RT (1985). A simplification of the Zoeppritz equations: Geophysics, 50:609–614.

Smith JC, Gidlow PM (1987). Weighted stacking for rock property estimation and detection of gas. Geophys. Prospecting 35:993–1014.

Spratt RS, Goins NR, Fitch TJ (1993). Pseudo-Shear—The Analysis of AVO in Castagna, J.P., and Backus, M.M., Eds., Offset-dependent Reflectivity-Theory and Practice of AVO analysis: Soc. Expl. Geophys., 37-56.

Swan HW (1993). Properties of direct AVO hydrocarbon indicators in Castagna, J.P., and Backus, M.M., Eds., Offset-dependent Reflectivity-Theory and Practice of AVO analysis: Soc. Expl. Geophys. 78–92.

Veeken PCH, Rauch M, Gallardo R, Guzman E, Vila Villasenor R (2002). Seismic inversion of the Fortuna National 3D survey, Tabasco, Mexico. First Break 20:287–294.

Veeken Paul, Marianne Rauch-Davies (2006). AVO attribute analysis and seismic reservoir characterization. First Break 24:41-52.

Verm R, Hilterman F (1995). Lithology color-coded seismic sections: The calibration of AVO crossplotting to rock properties. The Leading Edge, 14(8):847-853.

Waters KH (1981). Reflection Seismology: A tool for energy resource exploration: John Wiley & Sons, Inc.

Zoeppritz K (1919). Erdbebenwellen VIII B, Über Reflexion ad Durchgang seismischer wellen durch Unstetigkeitsflachen: Göttinger Nach. 66-84.

academicJournals

Vol. 8(24), pp. 1307-1318, 30 June, 2013
DOI: 10.5897/IJPS2013.3923
ISSN 1992 - 1950 © 2013 Academic Journals
http://www.academicjournals.org/IJPS

International Journal of Physical Sciences

Full Length Research Paper

Potential reduction of concrete deterioration through controlled DEF in hydrated concrete

Samo Lubej[1] and Milan Radosavljevic[2]

[1]Faculty of Civil Engineering, University of Maribor, Smetanova 17, 2000 Maribor, Slovenia.
[2]School of Construction Management and Engineering, University of Reading, Whiteknights, P. O. Box 219, Reading, RG6 & AW, United Kingdom.

Accepted 21 June, 2013

Delayed ettringite formation (DEF) is a chemical reaction with proven damaging effects on hydrated concrete. Ettringite crystals can cause cracks and their widening due to pressure on cracked walls caused by the positive volume difference in the reaction. Concrete may show improvements in strength at early ages but further growth of cracks causes widening and spreading through the concrete structure. In this study, finely dispersed crystallization nuclei achieved by adding air-entraining agent (AEA) and short vibration of specimens is presented as the main prerequisite for reducing DEF-induced deterioration of hydrated concrete. The study presents the method and mechanism for obtaining the required nucleation. Controlling long-term DEF by providing AEA-induced crystallisation nuclei, prevented excessive and rapid initial strength improvements, and resulted in a slight increase of compressive strength of fine grained concrete with only marginally lower density.

Key words: Delayed ettringite formation (DEF), aerated concrete, strength improvement.

INTRODUCTION

Delayed ettringite formation in cementitious materials is considered a harmful chemical reaction leading to a variety of damages (Diamond, 1996; Thomas, 2001; Barbarulo et al., 2005). The volume of the formed DEF crystals in the hardened concrete is larger than the volume of reactants and the main results are forces from the growing crystals acting upon walls of the crack. As a consequence, DEF cracks continue getting wider and spread through the concrete structure (Sahu and Thaulow, 2004; Thomas et al., 2008). In the study of DEF on railroad ties, Sahu and Thaulow (2004) found massive ettringite deposits at the interface between the paste and aggregate but with no signs of alkali-silica reaction, DEF was found to be the sole reason for map cracking. However, recent research has led to a better understanding of the mechanisms of DEF. It is believed that internal sulphate attack (ISA), which occurs in an environment free from external sources of sulphate, is the main mechanism that leads to DEF, particularly for heat-cured concrete structures (Collepardi, 2003).

In general, it is acknowledged that DEF is a result of a number of factors and conditions including excessive temperatures of above 70°C, the presence of sulfates, existing cracks, moist conditions etc (Taylor, 1990; Lawrence, 1995a, b; Ekolu et al., 2007a). Ekolu et al. (2007b) summarise various control measures that could be used for prevention of DEF, including the use of chemical additives. However, preventative measures and improvements in general durability require further attention.

In practice concrete and mortar mixes are normally based on Portland cement clinker, where the chemical process of hydration of clinker minerals yields hydrates and hydroxides. Because of the presence of gypsum, the

*Corresponding author. E-mail: samo.lubej@um.si. Tel. +386 2 2294333, Fax. +386 2 2524179.

chemical reaction between tricalcium aluminate (C_3A), gypsum ($CaSO_4$, $2H_2O$) and water, forms ettringite crystals ($3CaO$, Al_2O_3, $3CaOSO_4$, $31H_2O$). The volume difference in this reaction is positive and ettringite crystals grows faster, quickly growing on the unhydrated cement particles, which can slow down the hydration (Swaddiwudhipong et al., 2002). The presence of ettringite in a liquid cementitious system is unproblematic but its formation or re-formation in already hydrated concrete can lead to extensive damages (Collepardi, 2003). Due to the resulting volume difference particularly in the presence of sulfates, an expansive force within concrete can cause its disintegration (sulfate corrosion). It is well known that cements with low C_3A content are more resilient to sulfate corrosion although this also depends on the form of C_3A (Mather, 1968). For instance, crystalline C_3A is more reactive than its amorphous version.

The positive volume difference as a result of early ettringite formation (EEF) in cementitious materials rich with $C_4A_3\bar{S}$ calcium aluminate sulphate (expansive cement) can be used to compensate for the shrinkage during drying (Collepardi, 2001). In this case $C_4A_3\bar{S}$ hydrates within a few hours or days producing uniform distribution of ettringite and homogeneous expansion of hardened concrete at early stages. However, it is less known that ettringite could be formed in hardened cementitious materials without causing the well documented damages, which could potentially lead to their controlled strengthening.

The formation of a new phase characterized by volume expansion for the purpose of strength improvement is well known in the mainstream material science literature (Mishnaevsky, 2007). Such strengthening is based upon the creation of the internal compressive stresses on the contact between the existing matrix and the new phase particles, and depends on their shape, size and overall dispersion (Clifton and Ponnersheim, 1994). The newly formed particles should be small, spherical and located sufficiently apart from each other to avoid overlapping stress fields. Strength improvement of the Al_2O_3 ceramics with finely dispersed ZrO_2 particles is one example of this kind of strengthening (Cutler et al., 1987; Marshall et al., 1991). Internal stresses in the Al_2O_3 matrix created by applying the external force trigger polymorphic transformation of a tetragonal crystalline structure of ZrO_2 into a monoclinic crystalline structure. Increased volume creates substantial compressive stresses in the matrix surrounding the transformed particles leading to a several fold increase in compressive strength as well as resistance to the spreading of cracks. Studies that apply mechanisms of this kind for strength improvement of concrete are rare (Sobolev et al., 2006).

The creation of internal compressive stresses around particles or nuclei that have been transformed is the key requirement for such transformational strengthening. Its intensity depends on particle morphology, size and dispersion. Ideally, the particles should be small, spherical and uniformly dispersed to avoid overlapping their stress fields.

MATERIALS AND METHODS

In this study, the authors provide an investigation of a type of controlled DEF that may prevent deterioration or perhaps improve mechanical properties of hydrated fine grained concrete. A microstructure where crystallization nuclei are formed as a result of adding finely dispersed air-entraining agent (AEA) is the key prerequisite for such improvements. It is assumed that this would lead to localized and controlled formation of ettringite crystals, which could prevent DEF-induced deterioration. Their size and distribution depends on the level of dispersion of added AEA. The formation of localized ettringite crystals in the nuclei, particularly those adjacent to cracks, creates beneficial internal compressive stresses as the ettringite fills the nuclei. Similar to strength improvement of the Al_2O_3 ceramics described above, these internal compressive stresses lead to closure of nearby cracks preventing the growth of ettringite crystals. Furthermore, Ryu and Otsuki, (2002) show that the closure itself is beneficial since it decreases concrete permeability.

On the whole the experiments were based on fine grained concrete mixes using one type of cement, one type of AEA, fly ash and sand according to EN 196-1. Water-cement ratio, quantities of additives and hydration conditions were determined through laboratory testing. In addition, the experiments were based on specific climatic conditions necessary to achieve a controlled DEF in hydrated concrete. The investigation was based on four Portland cement (PC) CEM I 42, 5 R fine grained concrete mixes presented in Table 1.

The objective of this study is to investigate whether controlled DEF could lead to the reduction of deterioration and potential strengthening of hydrated fine grained concrete. To achieve this objective the study involves the following methods:

(1) Exposing hardened fine grained concrete prisms from the mix BI to the Duggan's test (Grabowski et al., 1992) (that is, prisms BI-DT); the test is essentially a cyclical interplay of heating and humidity and consists of a number of phases: prisms were first immersed in demineralised water for 72 h at 20 ± 2°C followed by 24 hours of drying in a drying chamber at 81 ± 2°C; they were then again immersed in the demineralised water for 24 h at 20 ± 2°C before being subject to 24 h drying in the chamber at 81 ± 2°C; in the last phase, prisms were immersed in the demineralised water for 24 h at 20 ± 2°C and then dried in the chamber for 72 h at 81 ± 2°C; the prisms were laboratory conditioned for 48 h in desiccators in between each of the above phases, and were once again immersed in the demineralised water for 24 h in order to fill the capillaries and voids with water,
(2) Strength comparison between hardened concrete prisms from mixes A, B, BI and prisms from mix BI that were exposed to the Duggan's test,
(3) Measuring ettringite formation by monitoring the length change (expansion) with a digital micrometer,
(4) microstructure comparison between hardened fine grained concrete samples from mixes A and AI where ettringite crystals were not detected with samples that were exposed to Duggan's test using electronic microscopy (that is, samples B-DT and BI-DT),
(5) Chemical analysis of ettringite crystals from samples B-DT and BI-DT in order to determine mass and atomic quantities of individual elements.

Four different mixes (A and AI, B and BI) were used for

Table 1. The four fine grained concrete mixes under investigation.

Parameter	Mix A (g)	Mix AI (g)	Mix B (g)	Mix BI (g)
Water	250	218,2	225	218,2
PC	450	450	310	310
Fly ash	-	-	140	140
AEA	-	6,8	-	6,8
Standard sand EN 196-1	1350	1350	1350	1350

Table 2. Results of the laboratory analysis for fly ash components.

Component part	Content (%)
Loss on ignition	0.41
Insoluble residue	16.67
SiO_2 impure	13.08
SiO_2 pure	47.62
SiO_2 soluble	0.64
SiO_2 total	48.26
SiO_2 active	35.18
Cao active	7.56
SO_3	1.88
CaO free	2.00

Figure 1. Apparatus for the measurement of length change of hardened concrete according to ASTM C490-86 placed in a climatic chamber.

comparative purposes because variations carried on:

(1) AEA content (A and B without AEA, versus AI and BI with AEA)
(2) Fly ash content (A and AI without fly ash versus B and BI with fly ash).

The comparison is necessary to identify the potential impact AEA and fly ash may have on mechanical properties before the prisms are exposed to Duggan's test (e.g. undesirable loss of compressive strength).

The above fine grained concrete mixes were prepared using a laboratory mixer according to EN 196-1. The conformity of fly ash for concrete was tested according to EN 450-1. The laboratory analysis of components presented in Table 2 confirmed that the fly ash used fulfils the criteria set in EN 197-1. Prisms were cast using 40 × 40 × 160 mm steel moulds. The samples from the mix B without AEA were then vibrated for 120 seconds with a standard low frequency of 50Hz and amplitude of 0.75 mm. The AEA-based samples from mixes AI and BI were vibrated for only 5 seconds under the same standard vibrating conditions as mix B samples in order to keep the volume of entrained air at an acceptable level (that is, preventing excessive reduction of strength). Past research shows that AEA-based samples should be vibrated with caution. For instance, Crawley (1953) found that high-frequency vibration causes more rapid loss of entrained air than moderate or low frequency vibration, and Hover (2001) reports that excessive vibration may lead to a complete loss of entrained air.

On the other hand, it has been found that short vibration cycles can improve compressive strength of concrete (Ozyldirim and Lane, 2003). A much shorter low-frequency vibration was therefore adopted to avoid a complete loss of finely dispersed crystallisation nuclei required for the controlled DEF. Controlled DEF is achieved by providing space for growth of ettringite crystals in the AEA-induced nuclei without any harm to hardened concrete. Specific climatic conditions were achieved by curing all prisms for 28 days in a climatic chamber at a temperature of 20±2°C and relative humidity of 98±2%. After a required 28-day curing period six prisms from each of the mixes B and BI were exposed to Duggan's test in order to achieve the accelerated ettringite formation. The prisms were then placed into a standard apparatus for the determination of length change of hardened cement paste, mortar and concrete, constructed according to ASTM C490-86. During these measurements the apparatus itself was placed in the climatic chamber with a constant temperature of 20±2°C and relative humidity of 98±2% shown in Figure 1.

Ettringite formation was then monitored by measuring length change (expansion) with Mahr's MarCator 1080/12.5/0.005 mm digital micrometer. The results were recorded with an analogue/digital converter connected to a workstation. Developing expansion was measured regularly in 15 m intervals with a measurement accuracy of 0.005 mm, although intervals could well be longer considering the slow pace of DEF.

Density of hardened fine grained concrete (ρ), its compressive (f_c) and flexural strength (f_m) were measured on 10 additional prisms for each of the three mixes after standard 7, 14 and 28 days, and additionally after 56 and 121 days when compressive and flexural strengths should reach a plateau. Mechanical properties of fine grained concrete were examined with a universal dynamometer and a method according to EN 196-1. Optical microscopy using OLYMPUS SZX stereo microscope and QUANTA 200 3D electronic microscope was used to monitor the microstructure development in the hydrated fine grained concrete. The use of the latter enables longer low-vacuum observations without gold or carbon coating of samples. Chemical analysis of reactants in the hydrated paste was performed with Line Scan Microscopy (LSM) using SIRION 400 NC scanning electron microscope that works at high-vacuum but

Table 3. Densities and mechanical properties of hardened fine grained concrete (mix A).

Time interval (days)	ρ (kg/m^3)	f_m (MPa)	f_c (MPa)
121	1894	6.1	26.4

Table 4. Densities and mechanical properties of hardened fine grained concrete (mix AI).

Time interval (days)	ρ (kg/m^3)	f_m (MPa)	f_c (MPa)
7	1876	4.0	18.0
14	1904	4.4	21.8
28	1883	7.2	23.3
56	1885	7.3	23.5
121	1887	7.4	25.5

Table 5. Densities and mechanical properties of hardened fine grained concrete (mix B).

Time interval (days)	ρ (kg/m^3)	f_m (MPa)	f_c (MPa)
7	1860	3.2	11.9
14	1857	3.5	14.2
28	1868	3.9	17.4
56	1872	4.1	19.3
121	1866	5.6	22.1

Table 6. Densities and mechanical properties of hardened fine grained concrete (mix BI).

Time interval (days)	ρ (kg/m^3)	f_m (MPa)	f_c (MPa)
7	1801	2.7	11.6
14	1807	5.2	14.3
28	1803	4.1	17.7
56	1805	4.1	17.8
121	1818	5.6	21.0

specimens have to be dry and treated (carbon treatment in this case). The ettringite crystals were characterised with the Energy Dispersive X-Ray (EDX) spectroscopy using JEOL JSM 5610 scanning electron microscope operated at 20kV for single-point 100 s long EDX measurements.

RESULTS AND DISCUSSION

Tables 3, 4, 5 and 6 show measured densities, flexural f_m and compressive strength f_c of hardened fine grained concrete prisms for mixes A, AI, B and BI that were not exposed to Duggan's test. The compressive strength of AI (BI) prisms after 121 days is only 3.4 % (5 %) lower than that of prisms A (B), which indicates that loss of strength due to added AEA can be prevented with short low-frequency vibration. These results reveal that 5 s vibration of BI prisms was sufficient to achieve a minimum loss of mechanical properties, which is normally expected from added AEA. On the other hand, the short vibration interval prevents the loss of crystallisation nuclei that can be seen later in the text.

Tables 7 and 8 show measured densities and mechanical properties of hardened fine grained concrete prisms for mortar mixes B and BI, but this time after 121 days, and exposed to Duggan's test after 28 days. Flexural strength of prisms B-DT that were exposed to Duggan's test has almost doubled to 11.2MPa, and compressive strength has more than doubled as well. These substantial increases in strength were not expected but to some extent there are some parallels with a study by Zhang et al. (2008). The study show that growth of ettringite crystals in a limited space of microvoids

Table 7. Density and mechanical properties of hardened fine grained concrete (B-DT: mix B exposed to Duggan's test).

Time (days)	ρ (kg/m^3)	f_m (MPa)	f_c (MPa)
121	2211	11.2	60.4

Table 8. Density and mechanical properties of hardened mortar prisms (BI-DT: mix BI with Duggan's test).

Time (days)	ρ (kg/m^3)	f_m (MPa)	f_c (MPa)
121	1810	6.0	22.4

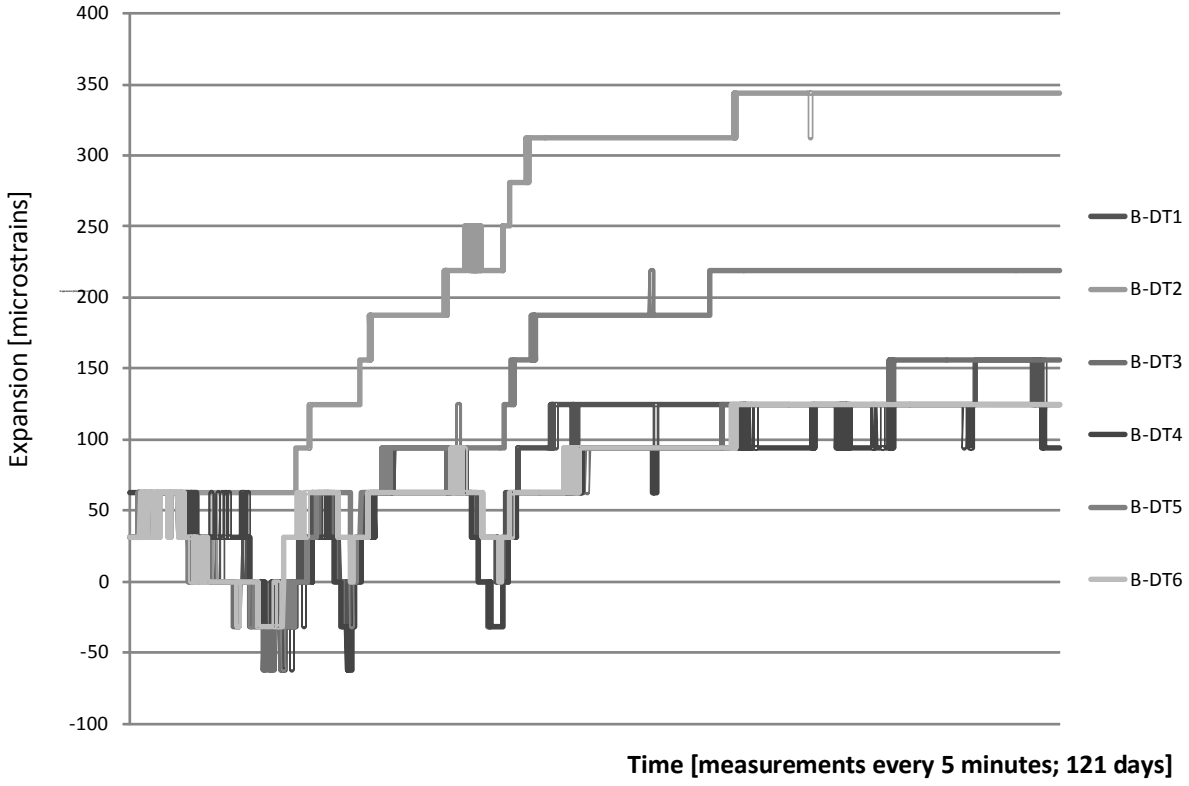

Figure 2. Change of length of six B-DT mortar prisms after the Duggan's test.

or preformed microcracks may lead to further evolution of localised microcracks. This process decreases the strength of prisms in early stages but ettringite crystals penetrate into the newly formed microcracks leading to partially recovered flexural strengths at later stages. One of the reasons for the increases could be associated with the increased ductility as a result of DEF-related expansion reported by Brunetaud et al. (2008). The observed causal relationship between tensile ductility and compressive strength has been observed in more detail by Bortolotti (1994). However, such increases are short-lived because the observed growth of ettringite crystals leads to the expansion at later stages, causing further cracking and deterioration of concrete.

Figures 2 and 3 show change of length for the six fine grained concrete prisms from the mixes B and BI that were exposed to Duggan's test and a final 24 hour immersion in demineralised water. The change of length of prisms was recorded daily and stopped after 93 days when measurements did not show any further expansion.

Comparing microstructures of the specimens from fine grained concrete mixes A, AI, and BI presented in Figure 4a, b and c demonstrate that, as expected, similar AEA-induced nuclei exist in AI and BI specimens.

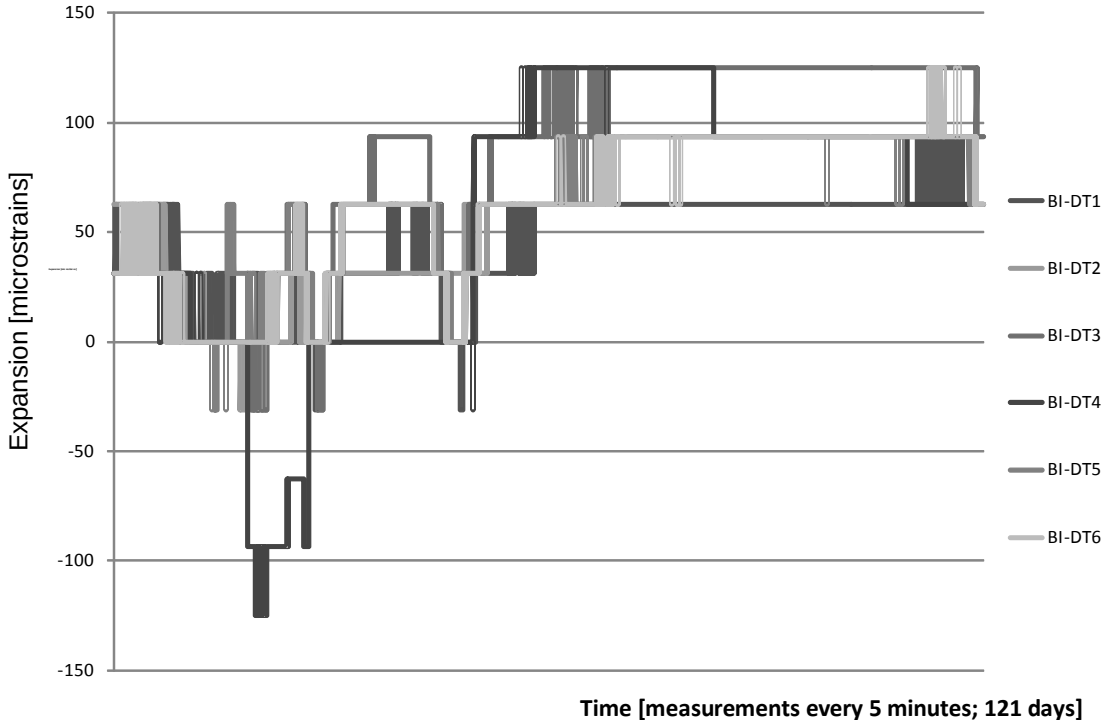

Figure 3. Change of length of six BI-DT fine grained concrete after the Duggan's test.

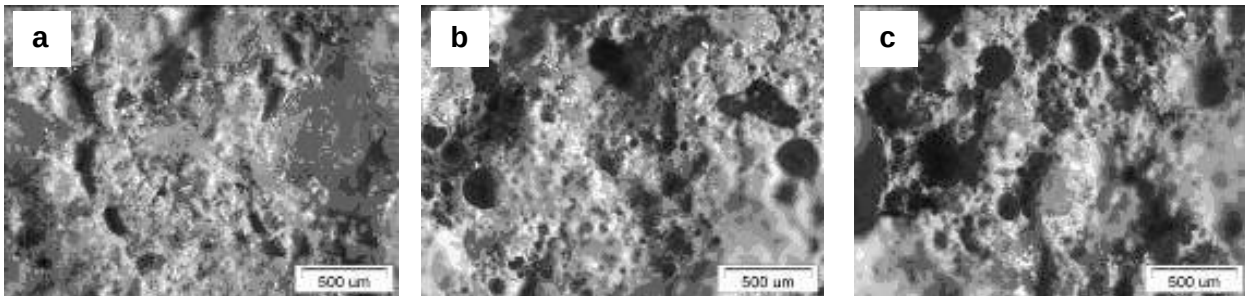

Figure 4 (a, b, c). Microstructures of fine grained concrete A, AI and BI after 121 days (500x magnification in all three cases; images obtained with OLYMPUS SZX stereo microscope).

Although ettringite crystals can be found in concretes produced by using pure Portland cement, no visible ettringite crystals were detected in any of the large number of prisms from the mix A. Ettringite crystals did appear in specimens of all other fine grained concrete mixes. Microstructures of specimen from the fine grained concrete mix AI show no visible ettringite crystals in AEA nuclei themselves displayed in Figure 5a, but they were detected in microcracks as seen in Figure 5b and c. Similar to Myneni et al. (1997) these crystals have thin, needle-shaped morphology and are approximately 2 µm in length revealing rapid growth. Fly ash in fine grained concrete mix BI may well be a source of soluble calcium for ettringite formation (Solem and McCarthy, 1992; Zhang and Reardon, 2003; Chrysochoou and Dermatas, 2006), because its crystals were found in greater quantities in microcracks and within the AEA-induced nuclei. Figure 6a, b, c and 7a, b, c, d, e, f show that ettringite crystals have thin, needle-shaped morphology but those found in microcracks are only approximately 2µm in length shown in Figure 7f, as opposed to 10 µm crystals found in the nuclei in Figure 6b.

The microcrack that appeared on the surface of a nucleous in Figure 7f can be associated with the shrinkage of the matrix during hydration (Stang, 1996). The comparison between various different BI specimen shows that ettringite crystals start growing wherever there is enough space for growth before further damaging

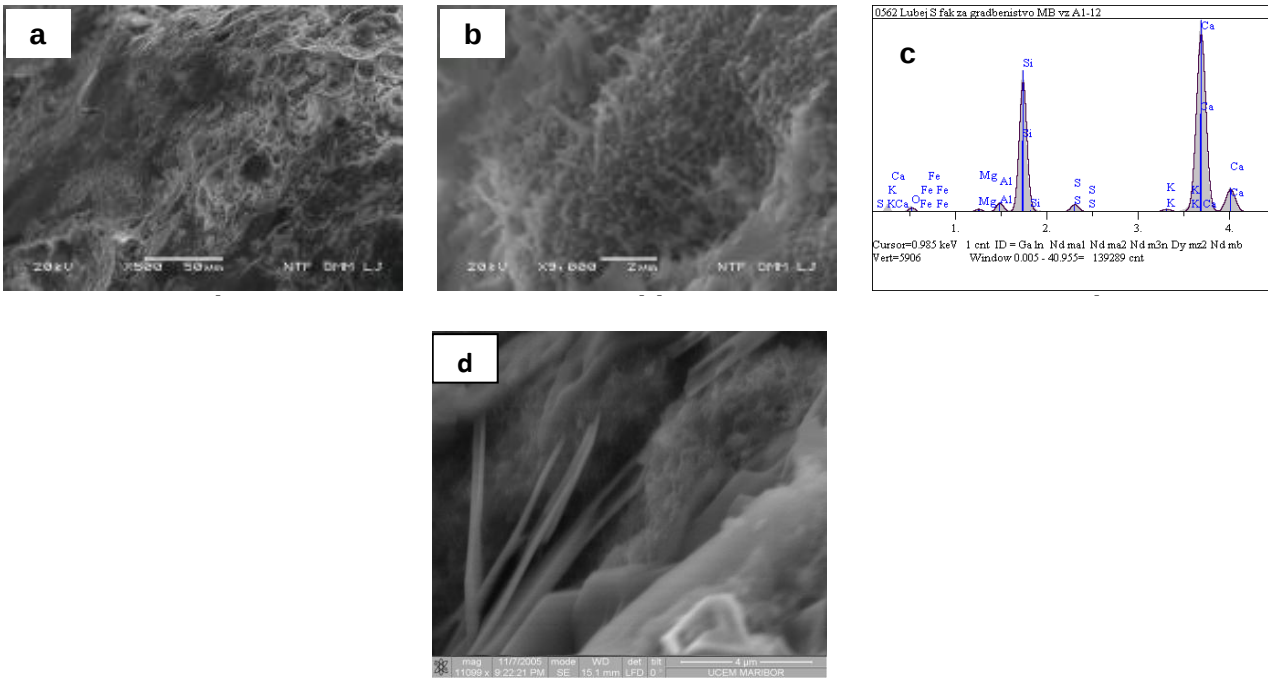

Figure 5 (a, b, c, d). Microstructure of fine grained concrete AI after 121 days (500x magnification in Figure 5a, and 9000x magnification of an area with thin approximately 2µm long ettringite crystals in figure 5b and 11000x magnification with QUANTA 200 3D electronic microscope in figure 5d; the results of the EDX analysis of a crystal from this area is in Figure 5c.

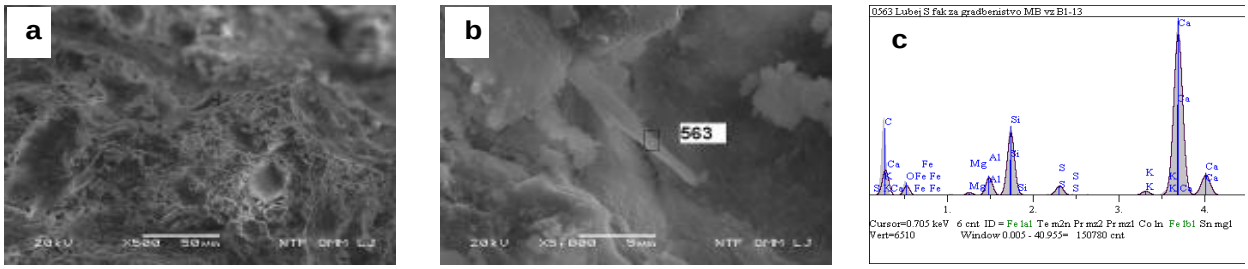

Figure 6 (a,b,c). Microstructure of fine grained concrete BI after 121 days (500x magnification in Figure 6a; the first studied area under 500x magnification of a nucleus with thin ettringite crystals with needle-shaped morphology and approximately 10um in length in figures 6b with the results of the EDX analysis of crystal 563 in Figure 6c).

concrete which enables further growth. AEA-induced nuclei may therefore act as relief reservoirs enabling the growth of substances like ettringite crystals in hardened concrete with minimum or no damaging effects. Hime, (1996) recommends air-entrainment as a way to prevent DEF and reports only a single incident where air-entrained concrete suffered from DEF.

Mix B has only been used to compare the microstructure and mechanical properties of specimen where fly ash has been added and the prisms were exposed to Duggan's test. Figure 8a reveals a microcrack in the B-DT sample at 500x magnification and Figure 8b clearly shows a cluster of up to 3 µm long ettringite crystals in the microcrack at 5000x magnification. Mehta (1983) reports that such type II crystals with the length of 1 to 2 µm and thickness of 0.1 to 0.2 µm are known to be more expansive and potentially more damaging than much longer - type I crystals. Because there are no AEA-induced nuclei DEF in B-DT samples increased microcracking giving space to further growth of ettringite crystals, which inevitably damage the hardened concrete. However, expansion of B-DT samples was not dissimilar to expansion of other samples. This may be assigned to a relatively short time interval since expansion was monitored for only 93 days after the Duggan's test.

Ettringite crystals growing in microcracks fill the empty space and press against their walls causing the DEF-induced expansion of concrete. As discussed earlier, this

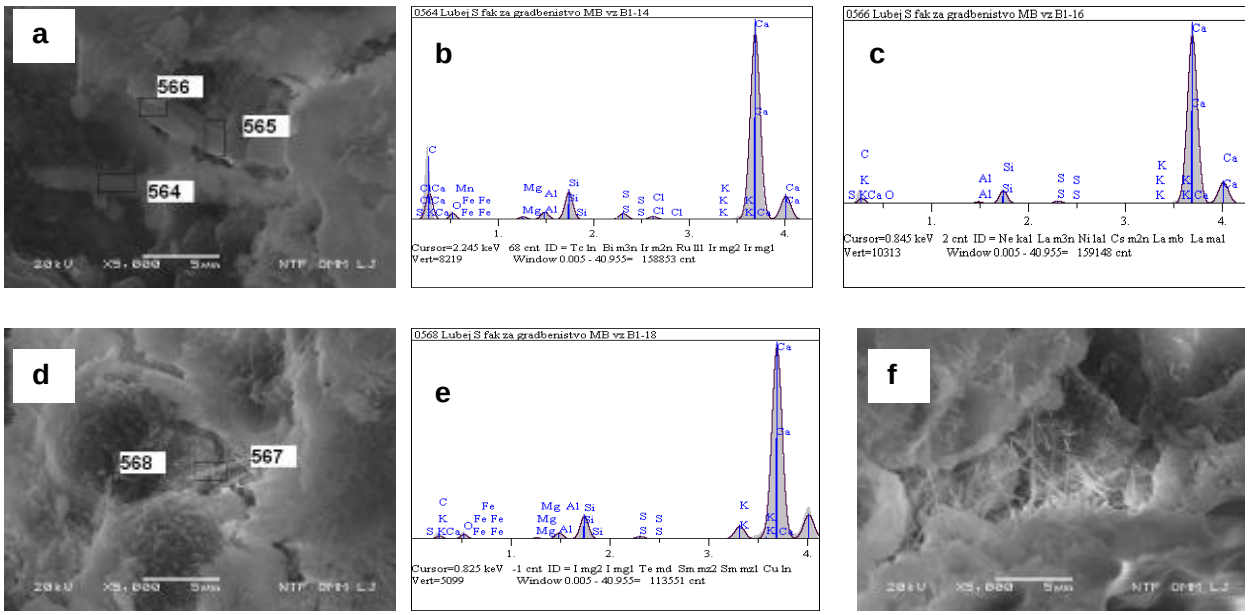

Figure 7 (a,b,c,d,e,f). Microstructure of fine grained concrete Bl after 121 days (the second studied area from figure 6a under 5000x magnification in Figure 7a,d and f; the results of the EDX analysis of crystal 564, 566 and 568 are in Figure 7b,c and e respectively).

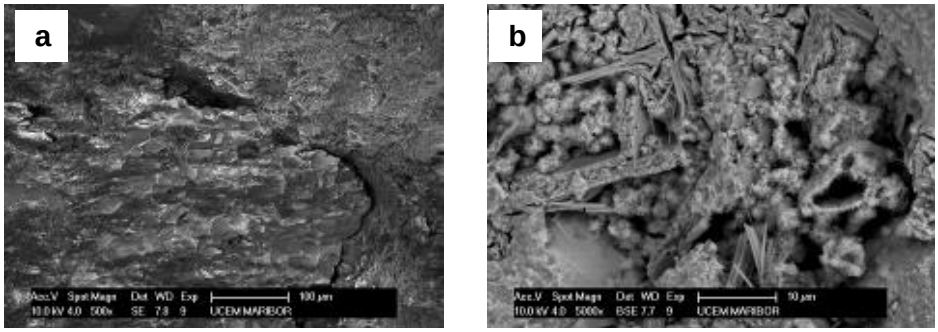

Figure 8 (a, b). Microstructure of fine grained concrete Bl after 121 days (500x magnification in figure 8a and 5000x magnification in Figure 8b; this mortar mix was used for comparative purposes only).

may in turn lead to initially improved mechanical properties before they are significantly reduced due to further evolution of growth-related microcracking. Compressive and flexural strength figures for B-DT samples after 121 days confirm this with compressive strength more than double the compressive strength of all other specimen. This improvement of mechanical properties is probably caused by ettringite crystals filling the empty space in existing microcracks before further evolution of localised microcracks that would significantly decrease the mechanical properties and damage concrete.

If DEF is limited to growth in microcrasks then specimens BI-DT that were exposed to Duggan's test should exhibit similar properties to B-DT specimens. Microstructure of the hardened fine grained concrete BI-DT after 121 days reveals visible ettringite crystals in AEA-induced nuclei in Figures 9b and 10b at 1,000 x and 5,000 x magnification respectively. These crystals are longer 10 µm type I crystals that are reportedly less damaging. The studied sections where AEA nuclei were present exposed some localised microcracking within the nuclei and presence of short ettringite crystals with needle-shaped morphology in the microcracks seen in Figure 11a and b. However, the majority of ettringite crystals were found within the nuclei themselves so the effect of their growth was assumed to be less damaging. Minimum expansion as shown in Figure 3 and comparable mechanical properties of specimens from all mixes, confirm this assumption.

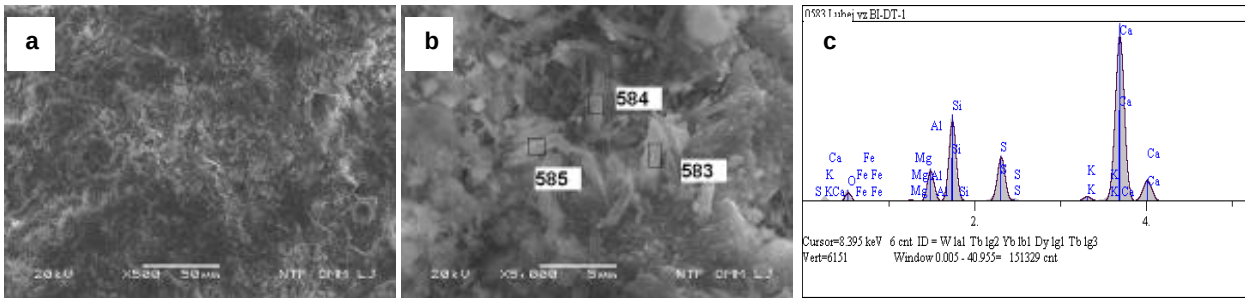

Figure 9 (a, b, c). Microstructure of fine grained concrete Bl after 121 days (500x magnification in Figure 8a with 5000x magnification of group crystals in the first studied area in figure 9b; the results of the EDX analysis of crystal 583 are in Figures 9c).

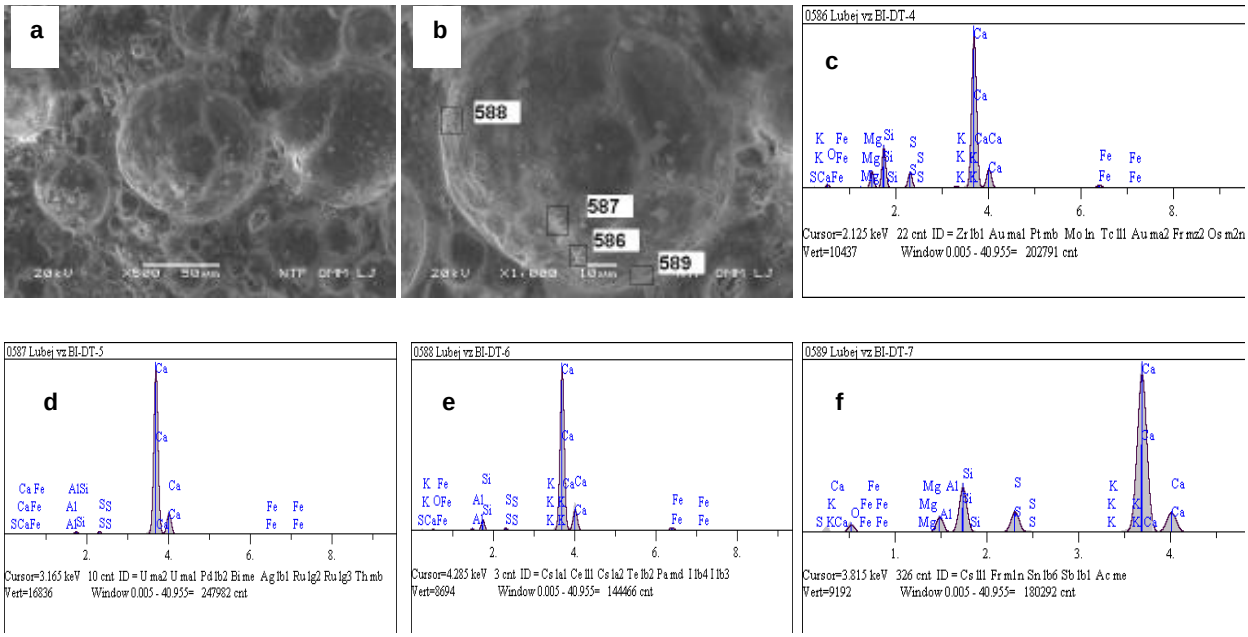

Figure 10 (a, b, c, d, e, f). Microstructure of fine grained concrete BI-DT after 121 days (500x magnification of a group of AEA-induced air voids in Figure 10a and 1000x magnification of an air void in Figure 10b; the results of EDX analysis of approximately 5 µm long crystals 586 and 587, and approximately 2 µm long crystals 588 and 589 are in Figures 7c, d, e and f respectively).

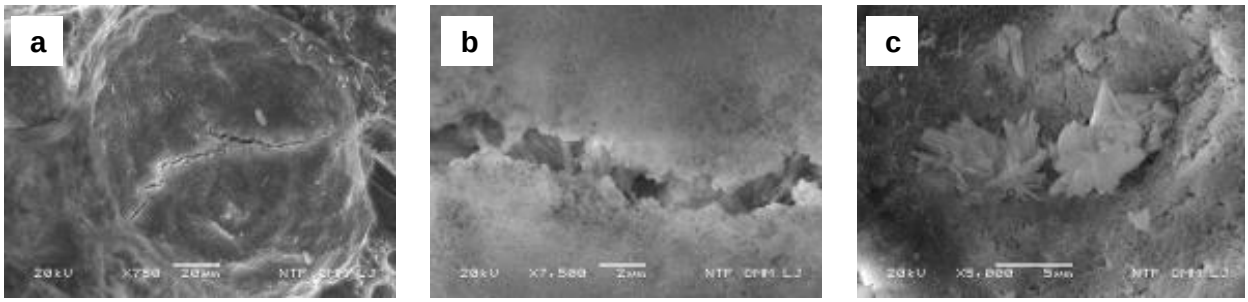

Figure 11 (a, b, c). Microstructure of fine grained concrete BI-DT after 121 days (750x magnification of an AEA nucleus with a microcrack in Figure 11a, 7,500x magnification of the microcrack in Figure 11b and 5000x magnification of the edge of the nucleus with a group of ettringite crystals in Figure 11c).

Table 9. Density and mechanical properties of hardened fine grained concrete without added AEA after 121 days for (prisms A, B and B-DT).

Variables	A	B	B-DT
ρ (kg/m^3)	1894	1866	2211
f_m (MPa)	6.1	5.6	11.2
f_c (MPa)	26.4	22.1	60.4

Table 10. Density and mechanical properties of hardened fine grained concrete with added AEA after 121 days for (prisms AI, BI and BI-DT).

Variables	AI	BI	BI-DT
ρ (kg/m^3)	1887	1818	1805
f_m (MPa)	5.6	5.6	6.0
f_c (MPa)	25.5	21.0	22.4

Table 11. EDX analysis results of the ettringite crystal at point 562 from sample AI in Figure 5c after 121 days.

Element	Mass %	Atomic %
Al	1.851	2.189
Si	26.567	30.187
S	1.740	1.732
Ca	55.105	43.878

The achieved compressive and flexural strengths of BI-DT specimens presented in Table 8 were similar to those of specimens B and BI in Tables 5 and 6 respectively and only 12% (15%) lower than those of specimens A(AI). The predominantly nuclei-based growth of ettringite crystals prevented excessive growth-related pressure on the walls of microcracks so no unusual initial improvements of mechanical properties were detected in the studied period. With a diameter of approximately 100 μm the nuclei offer sufficient space for ettrigite crystals to grow without causing progressive cracking and damaging the concrete.

Table 12.EDX analysis results of the ettringite crystal from the first studied area at point 563 from sample BI in Figure 6c after 121 days.

Element	Mass %	Atomic %
Al	2.975	2.280
Si	10.235	7.536
S	1.595	1.029
Ca	38.594	19.915

The EDX analysis was performed on a number of identified crystals to examine the presence of ettringite, which was confirmed in all cases. Tables 9-15 show compositions of studied ettringite crystals from Figures 5-11. The cement paste close to fly ash particles often contains CH crystals (Xu et al., 1993). It is therefore not unusual to see variations in Al/Ca and S/Ca ratios between different crystals that are presented in the tables. Wherever CH crystals are present Al/Ca and S/Ca ratios remain high (0.1-0.18 and 0.05-0.24 respectively). On the other hand, Al/Ca and S/Ca ratios are low at points where CH crystals are absent (0.01-0.05 and 0.01-0.04 respectively). Relatively high content of Si at some points follows high Al/Ca and S/Ca ratios in a similar way as shown by Richardson (2000). This could be associated with the availability of active SiO_2 in the fly ash although the values remain high even for specimens AI that do not contain fly ash. This, on the other hand, could also be associated with increasing concentrations of Si in the cement paste during hydration as reported by Rothstein et al. (2002).

Ettringite crystals have formed as a result of volumetrically expansive sulfate reaction in porous areas predominantly within AEA-induced nuclei, microcracks and microvoids in general. Because the solid product volume in this reaction is greater than the solid reactant volume, this has led to the creation of internal stresses in the ettringite growth areas. Their growth within the AEA-

Table 13. EDX analysis results of the ettringite crystal from the second studied area at points 564, 566 and 568 from sample BI in Figure 7b, c and e after 121 days.

Point	564		566		568	
Element	**Mass %**	**Atomic %**	**Mass %**	**Atomic %**	**Mass %**	**Atomic %**
Al	1.464	1.212	0.702	0.825	1.329	1.736
Si	5.077	4.038	4.347	4.907	4.696	5.896
S	1.034	0.720	0.836	0.827	0.467	0.513
Ca	49.763	27.735	80.577	63.744	50.309	44.269

Table 14. EDX analysis results of the ettringite crystal from the first studied area at point 583 from sample BI-DT in Figure 9c after 121 days.

Element	Mass %	Atomic %
Al	5.970	6.509
Si	15.727	16.473
S	9.340	8.568
Ca	47.938	35.185

Table 15. EDX analysis results of the ettringite crystal from the second studied area at points 586, 587, 588 and 589 from sample BI-DT in Figures 10c, 10d, 10e and 10f after 121 days.

Point	586		587		588		589	
Element	**Mass %**	**Atomic %**	**Mass %**	**Atomic %**	**Mass %**	**Atomic %**	**Mass %**	**Atomic %**
Al	4.875	5.783	0.225	0.328	0.831	1.109	3.958	4.260
Si	11.808	13.457	1.148	1.607	4.107	5.264	11.331	11.718
S	4.657	4.648	0.960	1.177	0.897	1.006	5.384	4.876
Ca	62.473	49.892	95.707	93.929	82.188	73.815	57.537	41.696

induced nuclei created compressive stresses within the concrete matrix that then led to strength improvements as suggested by Springenschmid and Breitenbucher (1998).

Conclusion

DEF has been detected in all fine grained concrete prisms that were exposed to Duggan's test (B-DT and BI-DT). In addition, non-aerated fine grained concrete prisms B-DT show rapid and excessive increases in compressive strength, which leads to known harmful damages of hardened, concrete. Controlling DEF by using AEA as a nucleation agent results in a slight increase of compressive strength of fine grained concrete with only marginally lower density (comparison between BI-DT and BI). The detected ettringite crystals within the crystallisation nuclei prevented initial improvements of mechanical properties, which were observed in fine grained concrete B-DT without AEA as a result of excessive growth-related pressure on the walls of microcracks. This could be one of the reasons why air-entrained concrete normally does not suffer from DEF as reported by Hime (1996). The investigation shows that AEA-induced nucleation can prevent deterioration of hardened concrete and may even offer a mechanism for improvement of mechanical properties but further investigations over longer test periods are required to establish whether the deterioration can be completely avoided and whether such improvements can be achieved and sustained.

REFERENCES

ASTM C490-86, Standard Specifications for Apparatus for Use in Measurement of Length Change Of Hardenet Cement Paste, Mortar, and Concrete, American Society of Testing and Materials, 1986.

Barbarulo R, Peycelon H, Prené S, Marchand J (2005) Delayed ettringite formation symptoms on mortars induced by high temperature due to cement heat of hydration or late thermal cycle, Cem. Conc. Res. 35(1):125-131.

Bortolotti L (1994). Influence of concrete tensile ductility on compressive strength of confined columns, J. mater. civil eng. 6(4):542-564.

Brunetaud X, Divet L, Damidot D (2008). Impact of unrestrained Delayed Ettringite Formation-induced expansion on concrete mechanical properties, Cem. Conc. Res. 38(11):1343-1348.

Chrysochoou M, Dermatas D (2006). Evaluation of ettringite and hydrocalumite formation for heavy metal immobilization: Literature

review and experimental study, J. Hazardous Mater. 136(1):20-33.
Clifton JR, Ponnersheim JM (1994). Sulfate attack of cementitious materials: Volumetric relations and expansions. *NISTIR 5390*, US Department of Commerce.
Crawley WO (1953). Effect of Vibration on Air Content of Mass Concrete, ACI J. Proc. 49(6):909-920.
Collepardi M (2003). A state-of-the-art review on delayed ettringite attack on concrete, Cem. Conc. Composites 25(4-5):401-407.
Collepardi M (2001). Ettringite formation and sulfate attack on concrete. In: Proceedings of the 5th CANMET/ACI International Conference on Recent Advances in Concrete Technology, Singapore, pp. 27-39.
Cutler RA, Bright JD, Virkar AV, Shetty DK (1987). Strength improvement in transformation-toughened alumina by selective phase transformation, J. Am. Ceramic Soc. 70(10):714-718.
Diamond S (1996). Delayed ettringite formation - Processes and problems, Cem. Conc. Composites, 18(3):205-215.
Ekolu SO, Thomas MDA, Hooton RD (2007a). Dual effectiveness of lithium salt in controlling both delayed ettringite formation and ASR in concretes, Cem. Conc. Res. 37(6):942-947.
Ekolu SO, Thomas MDA, Hooton RD (2007b). Implications of pre-formed microcracking in relation to the theories of DEF mechanism, Cem. Conc. Res. 37(2):161-165.
EN 196-1:1999 Cement and concrete technology, Cements, Cement mortar, Compressive strength, Flexural strength, Compression testing, Bend testing, Compaction tests, Test equipment, Test specimens, Acceptance inspection, Conformity, Approval testing.
EN 197-1:2002 Cement – Part 1: Composition, specification and conformity criteria for common cements.
EN 450-1:2005 Fly ash, Concretes, Construction materials, Ashes, Chemical composition, Fineness, Density, Expansion (deformation), Marking, Quality control, Conformity, Sampling methods, Size classification, Defects, Statistical quality control, Power station waste aggregates.
Grabowski E, Czarnecki B, Gillott JE, Duggan CR, Scott JF (1992). Rapid test of concrete expansivity due to internal sulfate attack, ACI Mater. J. 89(5):469-480.
Hime WG (1996). Delayed ettringite formation – A concern for precast concrete? PCI Journal, July-August, 26-30.
Hover KC (2001). Vibration Tune-up, Conc. Int. 23(9):30-35.
Lawrence CD (1995a). Mortar expansions due to delayed ettringite formation. Effects of curing period and temperature, Cem. Conc. Res. 25(4):903-914.
Lawrence CD (1995b). Delayed ettringite formation: an issue? *Materials Science of Concrete*, vol. IV, American Ceramic Society, Ohio, USA, pp. 113-154.
Marshall DB, Ratto JJ, Lange FF (1991). Enhanced Fracture Toughness in Layered Microcomposites of Ce-ZrO_2 and Al_2O_3, J. Am. Ceramic Soc. 74(12):2979-2987.
Mather B (1968). Field and Laboratory Studies of the Sulphate Resistance of Concrete, Performance of Concrete-Resistance of Concrete to Sulphate and Other Environmental Conditions, Thorvaldson Symposium Proceedings, University of Toronto Press, Toronto, pp. 66-76.
Mehta PK (1983). Mechanism of sulfate attack on Portland cement concrete-another look, Cem. Conc. Res. 13(3):401-406.
Mishnaevsky L Jr (2007). Computational Mesomechanics of Composites, John Wiley. 74(12):2979-2987.
Myneni SCB, Traina SJ, Logan TJ, Waychunas GA (1997). Oxyanion behavior in alkaline environments: Sorption and desorption of arsenate in ettringite, Environ. Sci. Tech. 31:1761–1768.
Richardson IG (2000). The nature of the hydration products in hardened cement pastes, Cem. Conc. Composites, 22(2):97-113.
Rothstein D, Thomas JJ, Christensen BJ, Jennings HM (2002). Solubility behaviour of Ca-, S-, Al-, and Si-bearing solid phases in Portland cement pore solutions as a function of hydration time, Cem. Conc. Res. 32(10):1663-1671.
Ryu JS, Otsuki N (2002). Crack closure of reinforced concrete by electrodeposition technique, Cem. Conc. Res. 32(1):159-164.
Sahu S, Thaulow N (2004). Delayed ettringite formation in Swedish concrete railroad ties, Cem. Conc. Res. 34(9):1675-1681.
Sobolev K, Flores I, Hermosillo R, Torres-Martinez LM (2006). Nanomaterials and nanotechnology for high-performance cement composites, Proceedings of ACI Session on “Nanotechnology of Concrete: Recent Developments and Future perspectives”, November 7, Denver, USA.
Springenschmid R, Breitenbucher R (1998). Influence of constituents, mix proportions and temperature on cracking sensitivity of concrete. In Springenschmid R (1998). Prevention of thermal cracking in concrete at early stages. RILEM Report 15, E & FN Spon.
Swaddiwudhipong S, Chen D, Zhang MH (2002). Simulation of the exothermic hydration process of Portland cement, Adv. Cem. Res. 14(2):61-69.
Taylor HFW (1990). Cement Chemistry, Academic Press, London, England.
Thomas MDA (2001). Delayed ettringite formation: Recent developments and future directions, in: S. Mindess, J. Skalny (Eds.), Materials Science of Concrete VI, American Ceramics Society, Westerville, OH, 2001, pp. 435–482.
Thomas M, Folliard K, Drimalas T, Ramlochan T (2008). Diagnosing delayed ettringite formation in concrete structures, Cem. Conc. Res. 38:841-847.
Ozyldirim C, Lane DS (2003). Investigation of self-consolidating concrete, Transportation Research Board Annual Meeting, National Research Council.
Solem JK, McCarthy GJ (1992). Hydration reactions and ettringite formation in selected cementitious coal conversion byproducts, Mater. Res. Soc. Symposium Proc. 245:71-79.
Stang H (1996). Significance of shrinkage – induced clamping pressure in fiber matrix bonding in cementitious materials, Adv. Cem. Based Mater. 4(3):106-115
Zhang M, Jiang M, Chen J (2008). Variation of flexural strength of cement mortar attacked by sulfate ions. Eng. Fracture Mechan. 75(17):4948-4957.
Zhang M, Reardon EJ (2003). Removal of B, Cr, Mo, and Se from wastewater by incorporation into hydrocalumite and ettringite, Environ. Sci. Technol. 37(15):2947-2952.
Xu A, Sarkar SL, Nilsson LO (1993). Effect of fly ash on the microstructure of cement mortar, Mater. Structures 26(7):414-424.

academicJournals

Vol. 8(24), pp. 1319-1333, 30 June, 2013
DOI: 10.5897/IJPS2013.3963
ISSN 1992-1950 © 2013 Academic Journals
http://www.academicjournals.org/IJPS

International Journal of Physical Sciences

Full Length Research Paper

Dissolved and particulate trace elements' configuration: Case study from a shallow lake

Feza Karaer[1], Aslıhan Katip[1], Saadet İleri[1], Sonay Sarmaşik[1] and Nurcan Aydoğan[2]

[1]Department of Environmental Engineering, Görükle Campus, 16059, Uludag University, Faculty of Engineering-Architecture, Bursa, Turkey.
[2]Bursa Metropolitan Municipality-General Directorate of Water and Sewerage Administration (BUSKİ), Bursa Eastern Wastewater Treatment Plant, Küçük Balıklı, Osmangazi, Bursa,Turkey.

Accepted 17 June, 2013

Trace element distribution was monitored for Uluabat lake water polluted with point and non-point sources in Bursa. An examination of Zn, Cr, Ni, Cu, Pb, As, B concentrations during the study period indicated that the particulate phase at the bottom of the water column were high in regard to dissolved phase. The source of trace elements in the deeper parts of the water column was derived from the higher concentrations of suspended solids present. Storm conditions and resuspension process in the lake was targeted as the source of trace elements' configuration in the dissolved and particulate phases. Significant correlations were found among temperature, pH, organic matter percentage, suspended solids, chlorophyll-a and particulate trace elements parameters. Factorial Anova Analysis was performed to help to understand the effects of parameters on adsorption of trace elements. Decrease in water level, increase of pH, organic matter percentage and suspended matter were appeared responsible for the increase of dissolved and particulate trace elements concentrations in summer season. Especially Cr, Zn, Pb and Cd concentrations were detected higher than the standards of EPA and WHO. The concentrations of trace elements in water column have to be monitored and the external loading with heavy metals coming from point and non-point sources has to be reduced for the conservation of ecological values.

Key words: Trace elements, dissolved phase, suspended particulate matter, Lake Uluabat.

INTRODUCTION

Certain heavy metals and trace elements in the form of dissolved and suspended particulate matter can introduce easily into the sediment layer (Stumm and Morgan, 1996; Sigg et al., 1987). Dissipation of trace elements from the water column is originated by the cycles of major elements in lake as photosynthetic production, $CaCO_3$ formation, iron and manganese oxides, aluminium and silicates (Stumm and Morgan, 1996). The pH interval in natural waters is between 7 to 8.5 which is the most acceptable range for adsorption of trace element ions to hydroxides and organic particulates. The heavy metal cations are completely

*Corresponding author. E-mail: karaer@uludag.edu.tr. Tel: +90 224 294 2108; Fax: +90 224 442 82 43.

*This study is a part of PhD thesis of the second author accepted on 26.05.2010 by the Graduate School of Natural and Applied Sciences of Uludag University.

released under circumstances of extreme acidic conditions (Shukla et al., 2002). Temperature, pH, redox potential, organic matter, ion exchange processes and microbiological activity affect some characteristics of trace elements such as mobility and bioaccumulation properties (Filgueiras et al., 2004). International standard values are used for determination of the evaluation of heavy metal's toxicity. Values of WHO and EPA guidelines can be given as an example for the standards (Anonymous, 2006a, b). The study site is shallow Lake Uluabat. It is subject to the "Convention on Wetlands of International Importance, especially as Waterfowl Habitat" (the RAMSAR Convention), which was approved in Ramsar, Iran in 1971. It was selected as the study area due to the international importance of this lake. The surface area of the lake is 161 km^2 at maximum water level and 138 km^2 at minimum water level and its average depth is 3 m (Dalkıran et al., 2006). Lake Uluabat has been contaminated by domestic and industrial waste waters and polluted runoff waters resulting from rainwater for many years. Particular problems of the Lake are eutrophication (Akdeniz et al., 2011) and heavy metal pollution. There are 67 residential areas, factories, workplaces, agricultural operations and mines in the basin of the Mustafakemalpaşa (MKP) creek which feeds the lake (Dalkıran et al., 2006). Furthermore, the MKP creek carries a significant amount of suspended solids, which is linked to a 12% reduction in the surface area and the volume of the lake, recorded between 1984, 1993 and 1998 (Aksoy and Özsoy, 2002). One of the most important centers in the MKP Basin, Tavşanlı has a sewage system without any treatment facility and the wastewater of Tunçbilek Thermal Power Plant and lignite plant are discharged to Orhaneli creek after being physically treated. The sewage water of MKP creek, wastewater of the leather organized industrial zone with physical treatment, wastewater of 27 dairy and butchery plants are discharged to the MKP creek without any treatment. In addition, there are 16 residential areas along the creek. The domestic and industrial wastewater of Akçalar is discharged to Akçalar creek, and then finally to Uluabat Lake (Dalkıran et al., 2006). Uluabat, Atabay and Karaoğlan pumping stations is that some of the neighbouring residential areas and factories discharge their wastewaters into the drainage canals of State Hydraulic Works (SHW). Reverse current occurs in the Kocasu creek draining the lake, because of flow rate is increased by rainfall during winter. The Kocasu creek formed by the merging of the Nilüfer and Simav creeks carry pollutants into the lake.

The objective of this study is to examine the concentration of selected trace elements in dissolved and particulate phase at 8 stations in Lake Uluabat annually between May 2008 and 2009. In addition, it is aimed to evaluate the effects of pH, temperature, organic matter percentage, suspended solids, chlorophyll-a and electrical conductivity parameters against trace element adsorption.

MATERIALS AND METHODS

Study area and sampling

The water and sediment samples were taken once in a month for annually, between May 2008 and 2009 in order to observe seasonal differences. The samples were taken on the same day from 8 stations, which were selected according to their distances from the contaminant sources in the lake and their hydrodynamic characteristics. The sampling stations presented different degrees of pollution around the lake. The first station is located in the outflow of Lake Uluabat. The second station is located near to the Atabay pumping station. Whereas the third station represented the north part of the lake, the fourth station is located in the entrance of the Mustafakemalpaşa creek. The fifth station represented the southwestern part of Island Mutlu which is located in nearby of Eskikaraağaç village. The sixth station is situated between Island Mutlu and Gölyazı village. The seventh station is presented at the near of Eskikaraağaç village. The new planned highway would pass close to these villages and finally the eighth station is located at the near of Akçalar village. The coordinates of sampling stations were determined with GPS and are shown in the map (Figure 1) and in Table 1. Determination of coordinates was based on European 1950 UTM coordinate system by the help of Magellan XL handheld GPS.

Samples were taken from all the sampling stations at two heights within the water column. The water samples at 0.5 m below the surface were taken by using the precleaned dark polyethylene bottles (Nguyen et al., 2005; An and Kampbell, 2003; Katip, 2010; İleri, 2010) and the others were taken from the lake bottom (just above the layer of the sediment) by using a precleaned standard sampling device (Hydro-Bios brand), which can take samples along the depth. Samples were transferred into dark-colored polyethylene (PE) bottles that had been washed with HNO_3 and deionized water. During sampling in situ, Temperature (T), pH and Electrical conductivity (EC) were measured using a HACH brand Sension 156 device (Burton and Pitt, 2002; Katip et al., 2012a, b). Sediment samples were taken from the top 5 cm of the sediment with an Ekman sediment sampler (Hydro-Bios brand) and transferred to the laboratory in plastic bags (Burton and Pitt, 2002). Arm-length gloves were used during sampling (Nguyen et al., 2005). A 1-liter water sample was taken along the water column in order to determine the chlorophyll-a concentrations, which is known to be linked to suspended solid concentration. In summer, as the algae increases, the SS concentrations also increase (Stumm and Morgan, 1996). The samples were transferred into the laboratory in dark-coloured PE bottles (Parsons and Strickland, 1963).

Sample handling and analysis

Suspended solids were determined gravimetrically by filtering 100 ml sample through a pre-weighed Milipore filter paper (pore size of 0.45 µm) (APHA, 1998). After the 1 L of sampled water was filtered through a GF/C filter paper, chlorophyll-a concentrations were measured by extracting the filtered water in 90% acetone and then reading the results on a spectrophotometer at 665, 645 and 630 nm wavelengths (Parsons and Strickland, 1963). Percentage of organic matter of sediment was measured by incineration method. pH and conductivity parameters of sediment were measured by 1 : 10 sediment-water mixture (Radojevic and Bashkin, 1999).

For trace element analyses, the following procedures were implemented. Water samples were filtered through a Milipore filter paper with preweighed 0.45 µm pore-size. The filter papers were then put into precleaned petri dishes and stored in a freezer. The filtered water samples were acidified with 0.2% (v/v) concentrated nitric acid and kept in glass bottles cleaned with detergent, water,

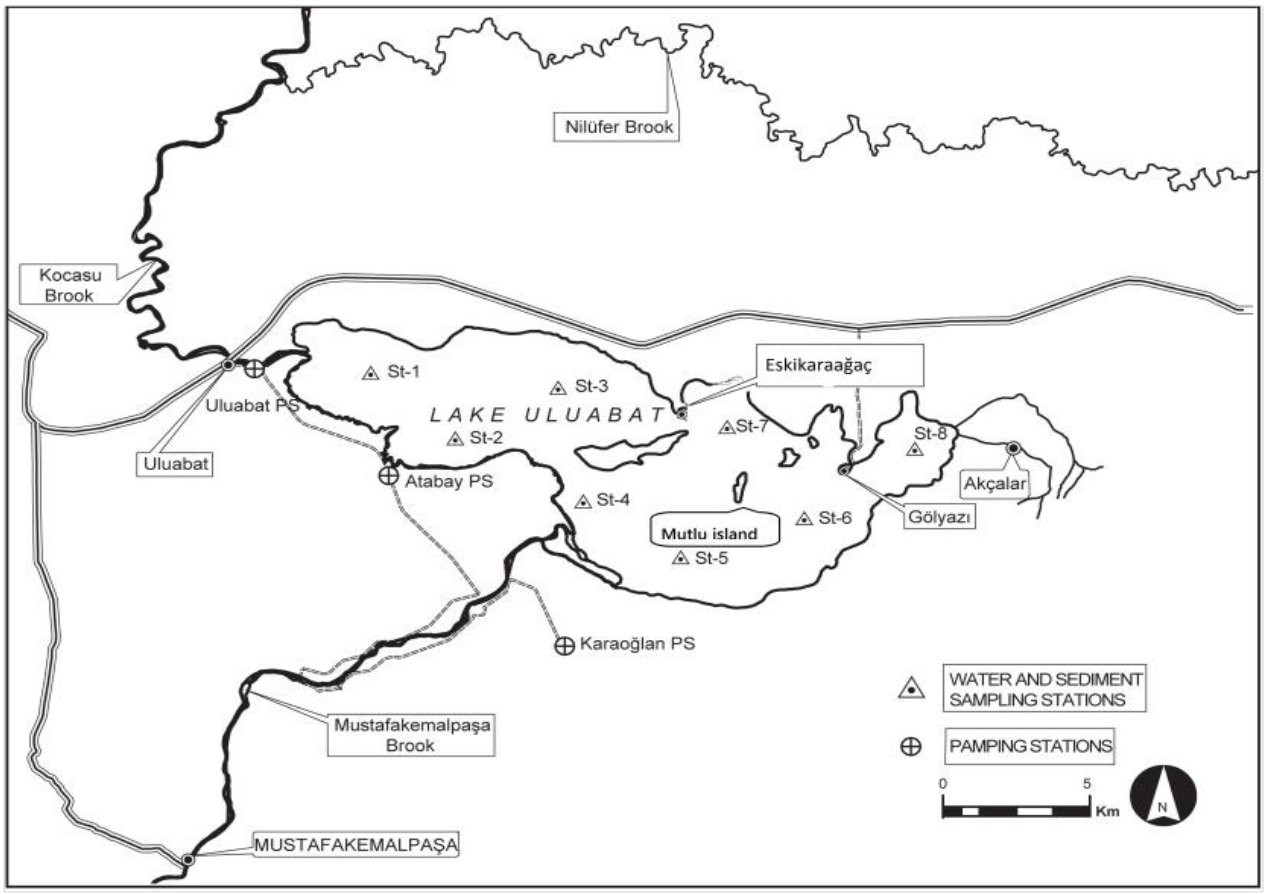

Figure 1. Sampling Stations in Lake Uluabat.

Table 1. The coordinates of sampling stations in Uluabat Lake.

Station No	X (East) (1950 UTM m)	Y (West) (1950 UTM m)
1	626865	4451240
2	629634	4448777
3	633217	4450699
4	633953	4446460
5	637299	4444284
6	641498	4445781
7	638853	4449214
8	645313	4448410

nitric acid and Mili-Q water respectively (An and Kampbell, 2003). The filter papers containing the suspended solids were air dried and reweighed again. They were digested with 4/1 (v/v) HNO_3/HCl mixture using a microwave device. After cooling, digestions were diluted to 30 ml with Mili-Q water. Samples were placed in Teflon cups and digestion operations were performed in a CEM brand Mars 5 model microwave device. Microwave decomposition operations were programmed as a 3-phase process. The device operated at 34.45 kPa for 1 min in the 1st stage, at 172.25 kPa for 5min in the 2nd stage and at 826.8 kPa for 60 min in the 3rd stage (Nguyen et. al., 2005). Trace elements were determined using the VISTA-MPX model of the VARIAN brand ICP-OES device. The operating conditions of the device, the wavelengths used in the detection of the elements and detection limits for analytical methods are shown in Tables 2 and 3 respectively (Anonymous, 2007a).

Three different groups were formed while preparing the standards in order to prevent elements from interfering with each other during detection. The grouping is as follows: 1st Group, Fe, Zn, Cr, Mn, Ni, Cu; 2nd Group, B, Cd, Pb; 3rd Group, As. The element As, in the 3rd group, was analyzed using a hybrid system. A standard stock solution of 1000 µg ml^{-1} (5% HNO_3) was used in the preparation of standards. As the concentrations of trace elements

Table 2. Operating conditions of the ICP-OES.

Parameter	
Power (kW)	1.2
Plasma flow (L min^{-1})	15
Auxiliary flow (L min^{-1})	1.5
Nebulizer flow (L min^{-1})	0.9
Replicate read time (s)	5
Instry stabilization delay (s)	30
Sample uptake rate (s)	40
Pump rate (rpm)	15
Rinse time (s)	10
Replicates	3
Display mode	Axial
Gas	Argon

Table 3. Wavelengths used in the detection of the elements.

Elements	Wavelength (nm)	Detection limit (µg L^{-1})
As	188.98	3
B	249.772	0.1
Cd	214.439	0.2
Cr	267.716	0.5
Cu	327.395	0.9
Fe	238.204	0.3
Mn	257.61	0.1
Ni	231. 604	0.7
Pb	220.353	1.5
Zn	213.857	0.2

dissolved and particulate in water are very different concentrations according to the each other, three different standard series (low, mid and high) were prepared at ppb level. The device was calibrated using a solution of 5 mg l^{-1} prepared from a Merck Mn solution of 500 mg L^{-1}. The ambient temperature was kept at 25°C to prevent possible expansion during the calibration (Anonymous, 2007a).

Statistical analysis of dissolved and particulate forms of trace elements in water was done. Correlation coefficients (r values) determine the correlations between parameters and p values show the significance levels. Factorial ANOVA Analysis was carried out by using General Linear Model method to be able to understand whether the differences of the trace element concentrations in the dissolved and particulate forms among stations, months and depth were significant. Study sample size is 192. All analyses were done in duplicate. The significance level was detected as p=0.05. All statistical calculations were done with Minitab 15.0 Program (Anonymous, 2007b).

RESULTS AND DISCUSSION

Dissolved trace elements

The concentrations of dissolved trace elements in the samples from Lake Uluabat varied between 0.0653 and 15.7298 mg L^{-1} (Fe), 0 and 0.1732 mg L^{-1} (Mn), 0.0011 and 1.3471 mg L^{-1} (Zn), 0 and 0.3508 mg L^{-1} (Ni), 0.0016 and 1.9597 (Cr), 0 and 0.3846 (Cd), 0 and 0.116 (Cu), 0.0012 and 0.0933 (As), 0.2253 and 5.5038 (B), 0 and 0.5028 mg L^{-1} (Pb), respectively. A comparison between the dissolved trace element concentrations found in Lake Uluabat and other fresh waters is presented in Table 4. It is seen that Fe, Zn, Cr, Ni, B and Pb concentrations in Lake Uluabat are higher than those of other water resources and other elements are within the similar ranges.

The degree of toxicity of dissolved metals according to their annual mean concentrations was evaluated with the help of international standards. Accordingly, As, Ni and B concentrations were found to be high according to standard values for potable water published by the World Health Organization (WHO) (Anonymous, 2006a) and low (except B) according to EPA guidelines (Anonymous, 2006b). Pb concentrations were found to be high according to WHO values and chronic effect values published by the EPA, and low according to the level of acute effect (Anonymous, 2006b). It was determined that mean Mn and Fe concentrations were below the standards. It was determined that Cd concentrations were higher than the standards of both WHO and EPA; Cu concentrations exceeded the chronic toxicity level and were very close to the acute level; Cr concentrations were higher than the chronic toxicity level; and Zn concentrations were higher than both the chronic and acute toxic limit values (Anonymous, 2006b). Table 5 shows the mean dissolved trace element concentrations in Lake Uluabat in comparison with international standard values.

Factorial ANOVA analysis of dissolved trace elements

Differences in the annual mean concentrations of dissolved trace element according to stations, depths and months; and differences in depths according to stations (interaction between station and depths) were examined using analysis of variance. The Factorial ANOVA results for dissolved trace elements are shown in Table 6. Analysis of variance showed significant differences between sampling stations in terms of Cr, Cd, Cu, Ni, B and Pb levels, and non-significant in differences between levels of As, Fe, Mn and Zn. The concentrations of Cr, Cu, Ni, B and Pb were highest at the 1st station, which is close to the outlet of the lake. The Kocasu creek which provides the outflow of the lake and reverse currents occasionally occur in it and Uluabat and Atabay Pumping Stations which are point sources of pollution are close to the 1st station. As the current in the stations 6, 3, 4 and 8 are faster than the other sampling locations, trace elements have a higher chance of being adsorbed to suspended solids and they are far from the pollution source. Trace elements concentrations were determined

Table 4. Dissolved trace element concentrations in Lake Uluabat and other fresh waters.

Elements	References	Mean ± SD
As (mg L^{-1})	Lake Texoma (An and Kampbell, 2003)	<0.033
	(Lake Uluabat)	0.023 ± 0.0179
B (mg L^{-1})	Lake Texoma (An and Kampbell, 2003)	0.225 ± 0.049
	(Lake Uluabat)	2.1668 ± 0.9964
Cd (mg L^{-1})	Lake Balaton (Nguyen et al., 2005)	0.000002
	River Vistula (Gue´guen and Dominik, 2003)	0.00056 ± 0.000018
	Lake Texoma (An and Kampbell, 2003)	0.020 ± 0.061
	(Lake Uluabat)	0.0116 ± 0.0427
Cr (mg L^{-1})	Lake Texoma (An and Kampbell, 2003)	0.004 ± 0.002
	River Vistula (Gue´guen and Dominik, 2003)	0.0013 ± 0.00005
	(Lake Uluabat)	0.0992 ± 0.2347
Cu (mg L^{-1})	Lake Balaton (Nguyen et al., 2005)	0.000475
	Lake Texoma (An and Kampbell, 2003)	0.024 - 0.020
	River Vistula (Gue´guen and Dominik, 2003)	0.03085 ± 0.0008
	(Lake Uluabat)	0.0115 ± 0.0142
Fe (mg L^{-1})	Lake Texoma (An and Kampbell, 2003)	0.119±0.093
	(Lake Uluabat)	0.5344 ± 1.3989
Mn (mg L^{-1})	Lake Texoma (An and Kampbell, 2003)	0.007 ± 0.018
	River Vistula (Gue´guen and Dominik, 2003)	0.35813 ± 0.00491
	(Lake Uluabat)	0.0116 ± 0.02
Ni (mg L^{-1})	Lake Texoma (An and Kampbell, 2003)	0.005 ± 0.003
	Lake Balaton (Nguyen et al., 2005)	0.0006
	(Lake Uluabat)	0.0304 ± 0.0448
Pb (mg L^{-1})	Lake Balaton (Nguyen et al., 2005)	0.00009
	Lake Texoma (An and Kampbell, 2003)	<0.015
	River Vistula (Gue´guen and Dominik, 2003)	0.00023 ± 0.00001
	(Lake Uluabat)	0.0355 ± 0.0567
Zn (mg L^{-1})	Lake Balaton (Nguyen et. al., 2005)	0.00085
	Lake Texoma (An and Kampbell, 2003)	0.059 ± 0.036
	River Vistula (Gue´guen and Dominik, 2003)	0.09225 ± 0.000966
	(Lake Uluabat)	0.1955 ± 0.2384

as minimum at these sampling stations. It was determined that while elements like Cu, Pb, Hg and Zn are affected by organic ligands, Cd formed a complex with inorganic ligands especially in muddy and summer conditions (Bradl, 2005). Highest Cd levels were found in the 2nd and 1st stations. The relation between the suspended solid substances and the trace elements was presented in Suspended particulate trace elements section.

The molar ratios of B:Fe:Zn:Mn:Cr:Ni:As:Cu:Cd:Pb are 200425:9160:2439:2238:1631:517:240:201:86:171 respectively and their order of size according to their concentrations was B>Fe>Zn>Cr>Pb>Ni>As>Cu>Mn>Cd, which were determined using their annual mean concentrations. Figure 2 shows the changes in the dissolved forms of Cr, Cd, Cu, Ni, B and Pb according to sampling stations. The concentration levels were observed to be low during

Table 5. Mean values of dissolved trace element concentrations in Lake Uluabat and international standard values (Anonymous, 2006 a, b).

Trace elements (mg L^{-1})	WHO	EPA, water quality criteria		Lake Uluabat
	Drinking water	CMC	CCC	
As	0,01 P	0.34 A,D,K	0.15 A,D,K	0.0182 ±0.0176
B	0,5 T			2.1668 ± 0.9964
Cd	0,003	0.002 D,E,K	0.00025 D,E,K	0.0097 ± 0.0371
Cr		0.57 D,E,K	0.074 D,E,K	0.0848 ± 0.2092
Cu	2	0.013	0.009 D,E,K	0.0128 ± 0.0141
Fe			1	0.5116 ± 1.2313
Mn	0,4 C			0.0123 ± 0.0217
Ni	0,02 P	0.47 D,E,K	0.052 D,E,K	0.0304 ± 0.0416
Pb	0,01	0.065 D,E	0.0025 D,E	0.0355 ± 0.0567
Zn		0.12 D,E,K	0.12 D,E,K	0.1595 ± 0.2169

CMC, Acute; CCC, Chronic; P, Provisional value. It is known to be hazardous but there is limited data about its effects on health; T, Provisional data; The measured values are below the refinable level; A, Recommended criterion derived for As (III). Adopted for total As because it shows similar effects with As (V); D, Recommended water quality criterion, based on the criteria for aquatic organisms by use of a conversion factor (CF); E, Standard values measured as a function of the hardness in the water column; K, Adapted from the criteria developed for aquatic organisms in 1995.

Table 6. Factorial ANOVA results of dissolved trace elements.

Elements	Stations	Depths	Months	Stations*Depths
As	0.411	0.123	0 *	0.959
B	0 *	184	0 *	0.613
Cd	0.002 *	0.545	0.010 *	0.983
Cr	0.008 *	0.763	0.057	0.6
Cu	0.007 *	0.081	0 *	0.632
Fe	0.767	0.621	0.394	0.376
Mn	0.330	0.600	0.516	0.651
Ni	0.004 *	0.175	0.003 *	0.987
Pb	0 *	0.202	0.001 *	0.384
Zn	0.439	0.513	0 *	0.563

* $p < 0.05$.

rainy season with respect to arid season. The monthly variations were statistically significant for As, Cd, Cu, Ni, Zn, B and Pb, and non-significant for Cr, Fe and Mn.

The trace elements with significant variations in monthly concentrations had high concentrations in summer and at the beginning of autumn in September, when there is no rain, and low concentrations in spring, in mid autumn and in winter, when concentrations were diluted by the increased rainfall. While the highest value of Cu was observed in summer, its lowest value was observed in October. This may be because of rainfall increase during this month, transporting more suspended solids to the lake by surface flows. Because if the lake is shallow compared to the winter months it mixes more easily, thereby increasing adsorption. In contrast to other metals, B levels were highest in November. It is thought that this was due to the increase in the flow rate and runoff in this month because of the pollution sources and rainfall. The monthly variations in the levels of dissolved As, Cd, Cu, Ni, Zn, B and Pb are presented in Figure 3.

Stronger winds cause vertical mixing of bottom sediment within the water column. This promotes to bonding between dissolved trace elements and particulates. The annual mean concentrations of suspended solids at the surface and the bottom of the water column were 37.15 and 60.70 mg L^{-1}, respectively. According to Table 6, concentrations showed non-significant differences depending on regions and significant differences depending on sampling stations. Factorial ANOVA analysis showed non-significant variation between the concentrations of dissolved trace elements at the surface and the bottom layers of the

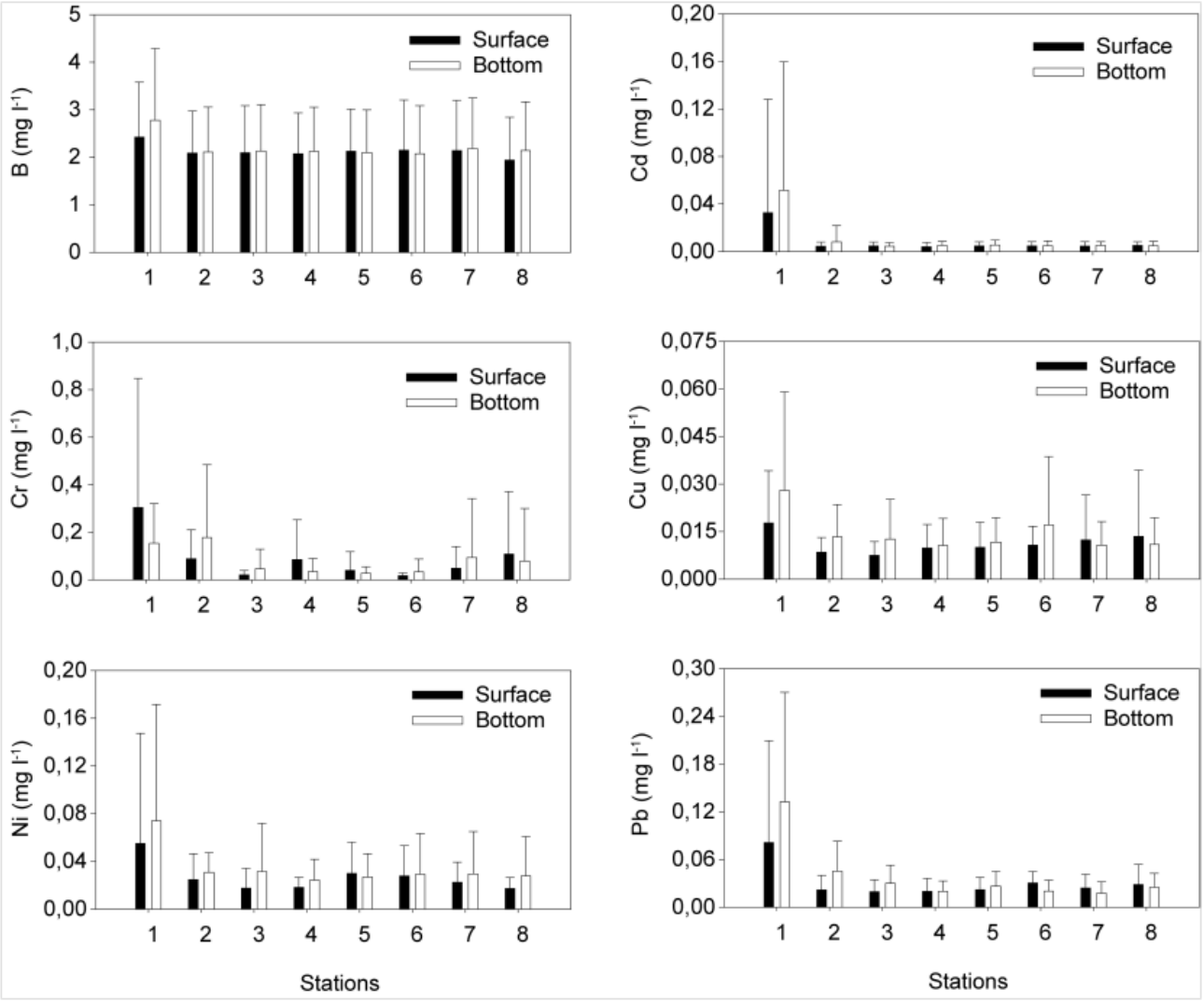

Figure 2. Variations in the concentrations of dissolved Cr, Cd, Cu, Ni, B and Pb according to sampling stations.

water column.

Suspended particulate trace elements

Factorial ANOVA analyses of suspended particulate trace elements

Table 7 shows annual means, standard deviations and concentration intervals of the particulate trace elements. In general concentration intervals are wide range. Adsorption-desorption mechanisms affected the particulate trace element concentrations within the suspended solids in the lake.

Factorial ANOVA was used to examine variations in the annual mean concentrations of particulate trace elements according to stations, surface and bottom distinction and season. Variations in Cr, Zn and B according to stations were found to be significant, and variations in the other trace elements were found to be non-significant. The maximum concentrations of Cr, Zn and B were observed at the 2nd, 3rd and 1st stations respectively. This may be because of those regions are exposed to a lot of wind and are also affected by the nearby SHW pumping stations, both of which cause water turbulence and increase the suspended solids concentration. The highest level of suspended solids (94.04 mg L^{-1}) was recorded at the 2nd station and the second-highest level of suspended solids (45 mg L^{-1}) was recorded at the 3rd station. Variations in the concentrations of particulate Cr, Zn and B according to sampling stations are shown in Figure 4. The statistical analysis showed that the variations in monthly means were significant for all of the elements. Therefore, the monthly variations in particulate trace elements are presented graphically in Figure 5. The annual mean of organic matter percentage in sediment

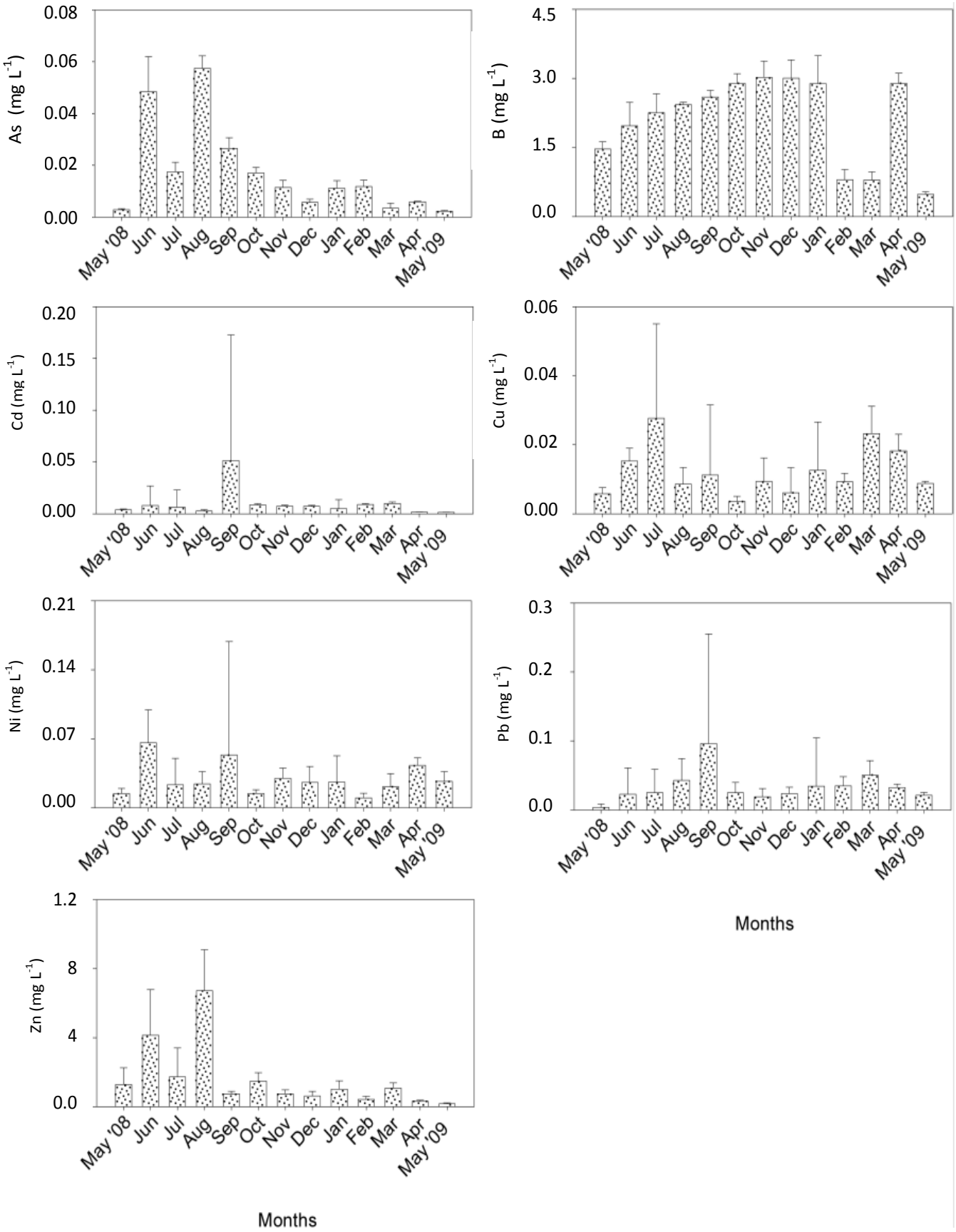

Figure 3. Monthly variations in dissolved As, Cd, Cu, Ni, Zn, B and Pb.

Table 7. Particulate trace element concentrations in Lake Uluabat and other fresh waters.

Elements	References	Min. - Max.	Mean ± SD
Cd (mg kg^{-1})	Changjiang and Hangzhou Bay (Che et. al., 2003)	0.04 - 8.39	0.565 ± 0.82
	Lake Balaton (Nguyen et al., 2005)	0.11 - 1.25	0.385
	River Danube (Yiğiterhan and Murray, 2008)		1.14
	Lake Uluabat	0 - 6.1877	1.1667 ± 0.5874
Cr (mg kg^{-1})	Lake Balaton (Nguyen et al., 2005)		19
	Lake Uluabat	0.0140 - 168.1396	13.4087 ± 20.2079
Cu (mg kg^{-1})	Changjiang and Hangzhou Bay (Che et al., 2003)	0.5 - 157.5	46.05 ± 25.6
	Lake Balaton (Nguyen et al., 2005)		16.5
	River Danube (Yiğiterhan and Murray, 2008)		115
	Lake Uluabat	0 - 49.9319	5.3701 ± 5.2744
Fe (mg kg^{-1})	Lake Balaton (Nguyen et al., 2005)	3700 - 27300	9950
	River Danube (Yiğiterhan and Murray, 2008)		36000
	Lake Uluabat	33.1149 - 26509.08	2039.2269 ± 2949.51
Mn (mg kg^{-1})	Lake Balaton (Nguyen et al., 2005)	199 – 12500	1300
	River Danube (Yiğiterhan and Murray, 2008)		1700
	Lake Uluabat	3.9596 - 565.8088	50.9093 ± 66.6561
Ni (mg kg^{-1})	Lake Balaton (Nguyen et al., 2005)		25
	Lake Uluabat	0.0161 - 123.9227	18.6455 ± 26.0972
Pb (mg kg^{-1})	Changjiang and Hangzhou Bay (Che et al., 2003)	2 – 175	32.5 ± 18.3
	Lake Balaton (Nguyen et al., 2005)		29.5
	River Danube (Yiğiterhan and Murray, 2008)		84
	Lake Uluabat	0 - 105.247	7.61223 ± 9.4288
Zn (mg kg^{-1})	Lake Balaton (Nguyen et al., 2005)	18-147	71.5
	River Danube (Yiğiterhan and Murray, 2008)		248
	Lake Uluabat	0.2246 - 162.4596	26.8742 ± 27.4318

was found to be 3.81% for the lake; this increased to 3.99% in summer and decreased to 3.55% in winter. The highest organic matter content for an individual sampling station was 4.2%, recorded at the 8th station. This station had the lowest values of Cr, Zn and B. Moreover, it was determined (Table 8) that the level of Zn is related to the percentage of organic substances in the sediment. When monthly variations of trace elements were examined, it was found that concentrations tended to increase in summer and in September while to decrease from the mid autumn to the end of spring in general.

This increase in summer was thought to occur as a result of elements transferred from the sediment to the water column, as a result of wind induced mixing (Bailey and Hamilton, 1997) and the decrease in dilution and the reduced water level. The transfer of elements from the sediment to the water showed a particular increase as a result of the increase in the solubility of metals as temperature increases, and elements bounded to the suspended solids again. Cd, Cu, Zn, As and B were found in high concentrations during rainy seasons. This may be resulted by the adsorption of those elements to solid substances which are increased with surface flows and then carried into the lake and by the amount of phytoplankton increases especially in spring (Straškraba et al., 1993).

The molar ratios of B:Fe:Mn:Zn:Ni:Cr:Cu:As:Cd:Pb, were37002:365145:9266:4110:3175:2606:845:127:103:3 67, respectively, which were determined by taking the annual mean of the particulate trace elements in the lake. Their order of size according to their concentrations was Fe>Mn>B>Zn>Ni>Cr>Pb>Cu>Cd>As. This differed from the size order of dissolved trace elements. A comparison of the concentrations of the particulate trace elements with the other fresh waters sources is presented in Table 7. According to this comparison, except for Cd, the concentrations of the other metals examined were at low levels. The reason is that Cd can form a complexation

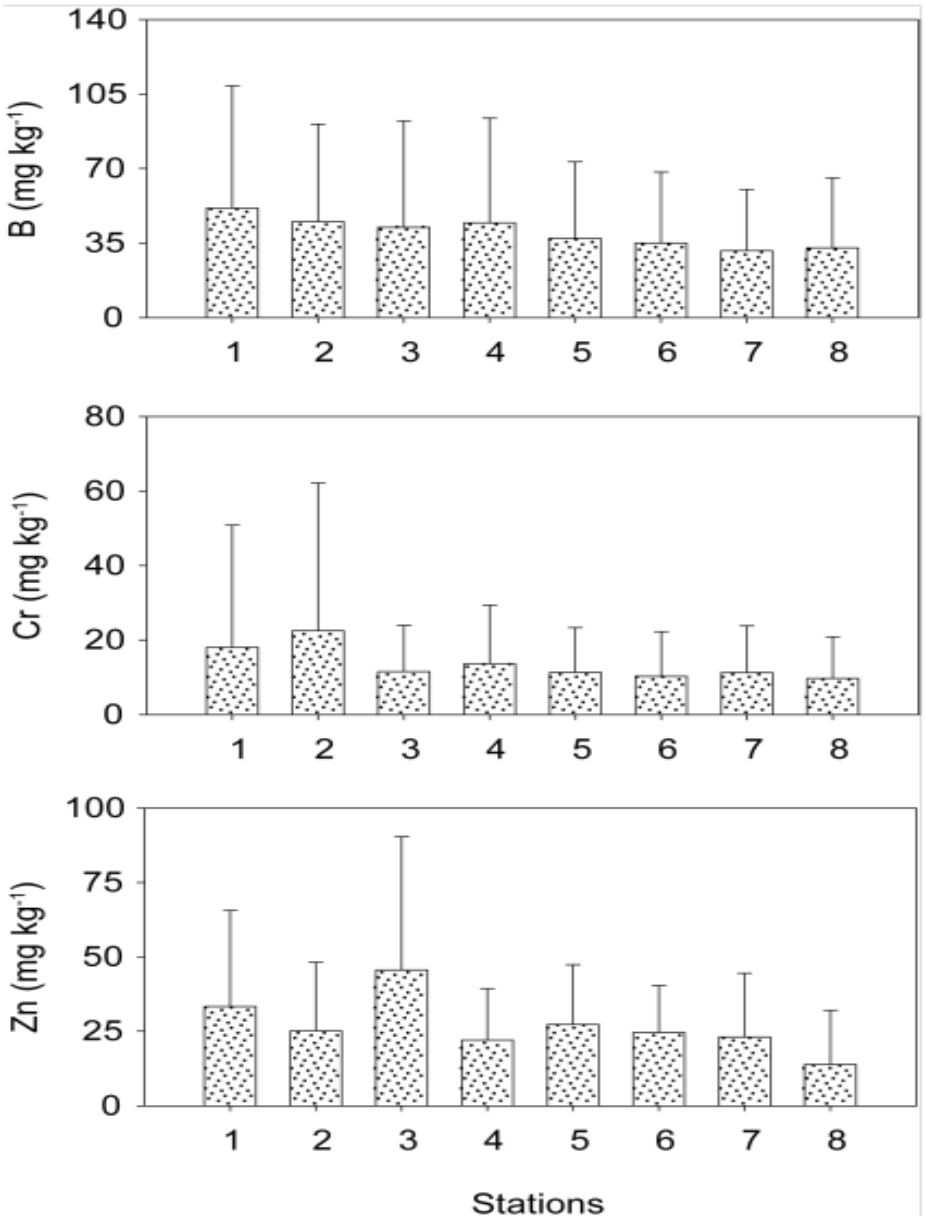

Figure 4. Variations in the concentrations of particulate Cr, Zn and B according to sampling stations.

with inorganic ligants in mudier and arable soils (Bradl, 2005). Therefore, Cd was accumulated in the mudier sediment layer of Uluabat lake. Concentration of particulate form of Cd was increased by flows in water and resuspension process. Some dissolved trace elements like Fe, Zn, Cr, Ni, B, Pb concentrations are higher than the water sources. Another reason is that heavy metals coming from point sources such as creeks and pump stations located around the lake are in dissolved form.

Factorial ANOVA analysis showed higher concentrations of particulate Cu, Ni, Fe and Mn within samples at the bottom of the water column compared to surface samples. The other elements showed non-significant variations between surface and bottom samples. This was resulted from the greater amount of suspended solids at the bottom of the water column and the relationship between chlorophyll-a and suspended solid concentrations. Due to these differences between surface and bottom concentrations, variation graphs of the particulate trace element concentrations were produced by calculating the surface-bottom means of each station. Figure 6 showed examples of concentration difference for particulate Cu and Fe at the surface and

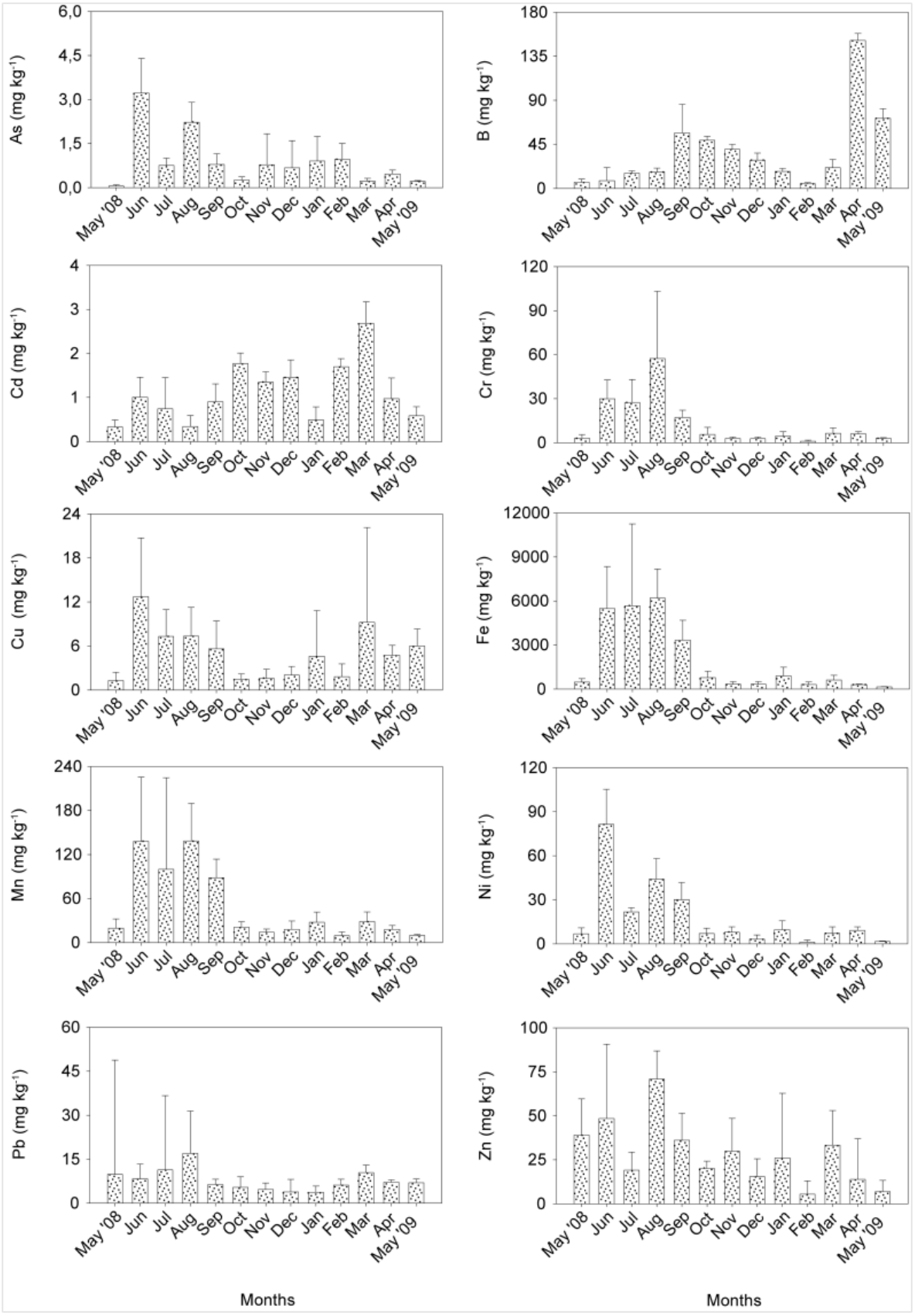

Figure 5. Monthly variations in particulate trace elements.

Table 8. The matrix of correlation coefficients (r-values) among particulate trace elements with water and sediment quality parameters.

	As	Cr	Cd	Cu	Ni	Fe	Mn	Zn	B	Pb	pH	T	EC	Chl-a	Organic Matter
Cr	0.414 *														
Cd	-0.21 *	-0.12													
Cu	0.203 *	0.288 *	0.012												
Ni	0.709 *	0.578 *	-0.196	0.428 *											
Fe	0.4 *	0.747*	-0.061	0.292 *	0.614 *										
Mn	0.445 *	0.731 *	-0.029	0.327 *	0.677 *	0.961 *									
Zn	0.359 *	0.436 *	-0.076	0.294*	0.447 *	0.363 *	0.37 *								
B	-0.33 *	-0.2	-0.136	-0.12	-0.23 *	-0.23 *	-0.226 *	-0.14							
Pb	0.272 *	0.318 *	-0.102	0.224 *	0.356 *	0.29 *	0.295 *	0.284 *							
pH	0.35 *	0.062	-0.039	-0.14	0.134	0.071	0.08	-0.07	-0.284 *	-0.142					
T	0.288 *	0.525 *	-0.3 *	0.385 *	0.589 *	0.524 *	0.505 *	0.287 *	0.083	0.382 *	-0.101				
EC	0.231 *	-0.01	-0.027	0.011	0.225 *	0.079	0.117	0.036	-0.096	-0.064	-0.099	0.099			
Chl-a	0.326 *	0.295 *	-0.112	0.278 *	0.509 *	0.398 *	0.445 *	0.047	-0.145	0.015	0.209 *	0.549 *	0.331 *		
Organic Matter	0.326 *	0.153	-0.067	0.192	0.361 *	0.158	0.191	0.362 *	-0.047	0.293	-0.014	0.335 *	0.303*	0.241 *	
SS	0.228 *	0.445 *	-0.033	0.21 *	0.614 *	0.519 *	0.607 *	0.237 *	-0.051	0.16	0.006	0.332 *	-0.008	0.445 *	0.116

*$p < 0.05$.

the bottom.

Relationship between the particulate trace elements and the water-sediment quality parameters

Relationship between the particulate trace elements and the Chlorophyll-a concentrations (Stumm and Morgan, 1996) were studied. The effects of temperature, conductivity and pH on trace elements are emphasised (Ikem et al., 2003). Dissipation of trace elements from the water column is realised with absorption to algae and precipitation. The decrease in pH and the increase in temperature affect the disssolution of metals (Fernández et al., 2000). Therefore, the relationships among organic matter percentage, temperature, pH and conductivity parameters in the sediment layer were analysed. Also, suspended solids, particulate trace elements and chlorophyll-a parameters in lake water were evaluated statistically. The results showed a significant relationship between all of the elements, except for Cd, which only showed a significant relationship with As. Particularly the correlation between Fe with Mn, Cr and Ni, and the relation of Mn with Cr and Ni, were found to be higher compared to the other correlations. This findings reflected that the movements of elements can be similar to each other. Significant relationships were found between temperature and all of the elements except B; between suspended solids and all the elements other than Cd, B and Pb; and between chlorophyll-a and all the elements other than Cd, Zn, B and Pb. The positive correlations were found between suspended solids and chlorophyll-a showing that elements can be adsorbed to solid substances. It was determined that the amount of organic matter percentage in the sediment was related with As, Ni, Zn and Pb; conductivity was related with As and Ni; and pH was related with As and B. It was thought that there may be transfer from the sediment to the water as a result of decomposition of organic matter and an anaerobic condition resulting from the increase in temperature, the percentage of organic matter and therefore the conductivity. The matrix of correlation coefficients (r - values) among particulate trace elements with water and sediment quality parameters are presented in Table 8 and the correlation graphs between particulate Cr, Ni, Fe Mn and suspended solids are presented in Figure 7.

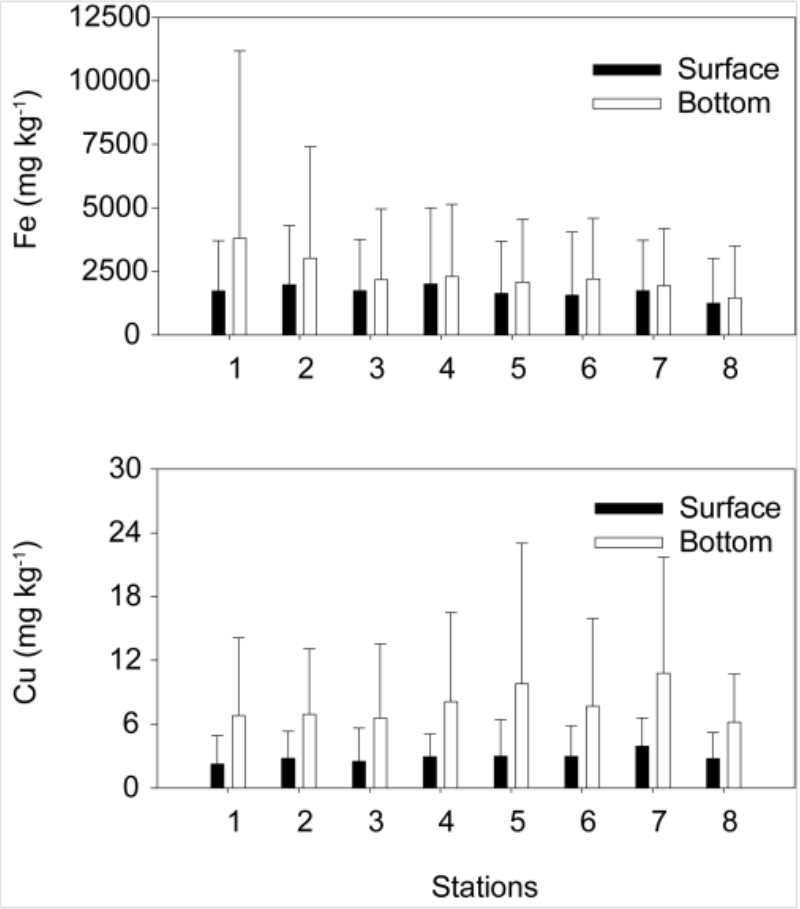

Figure 6. Surface and bottom concentrations of particulate Cu and Fe.

Conclusion

Dissolved and particulate trace elements concentrations were examined in lake water and sediment for 8 sampling stations representing the different regions of Lake Uluabat in Turkey. The dissolved and particulate trace elements concentrations were determined at the surface and the bottom layers within the water column. In general the highest concentrations of trace elements were observed in the particulate form. Lower organic content in water indicated that the suspended solids were transferred from the sediment. Concentrations of particulate Cr, Zn and B were detected lowest at the 8th sampling station where organic matter percentage in the sediment was highest.

The size of the trace elements according to the concentrations of the elements were B>Fe>Zn>Cr>Pb>Ni>As>Cu>Mn>Cd for the dissolved trace elements; and Fe>Mn>B>Zn>Ni>Cr>Pb>Cu>Cd>As according to particulate trace elements.

The differences between the surface and the bottom layers of the water column were non-significant in terms of dissolved trace elements, but significant in terms of some of the particulate trace elements (Fe, Mn, Cu and Ni). The concentrations of dissolved trace elements at the bottom of the water column were observed to be higher than those of surface samples. This difference was resulted from the higher concentrations of suspended solids present in the deeper parts of the water column.

Mostly, the dissolved and particulate trace elements were detected high in summer season. The main reason was the increase of concentrations of dissolved trace elements depending on solubility, decrease in water level and increase in air temperature. Furthermore, increase in photosynthetic production by implication of pH, concentration of $CaCO_3$ and adsorption capacity of iron and manganese oxides have caused this situation. In addition increasing wind velocity in summer season induced the mixing of sediment layer into the water column bringing about suspended trace elements. Significant correlations were found between suspended solids and particulate Fe, Mn, Zn, Cr, Cu, As, Ni elements; between Chl-a and particulate Fe, Mn, Cr, Cu, As, Ni elements. Same correlation was observed for particulate trace elements (except B) and temperature;

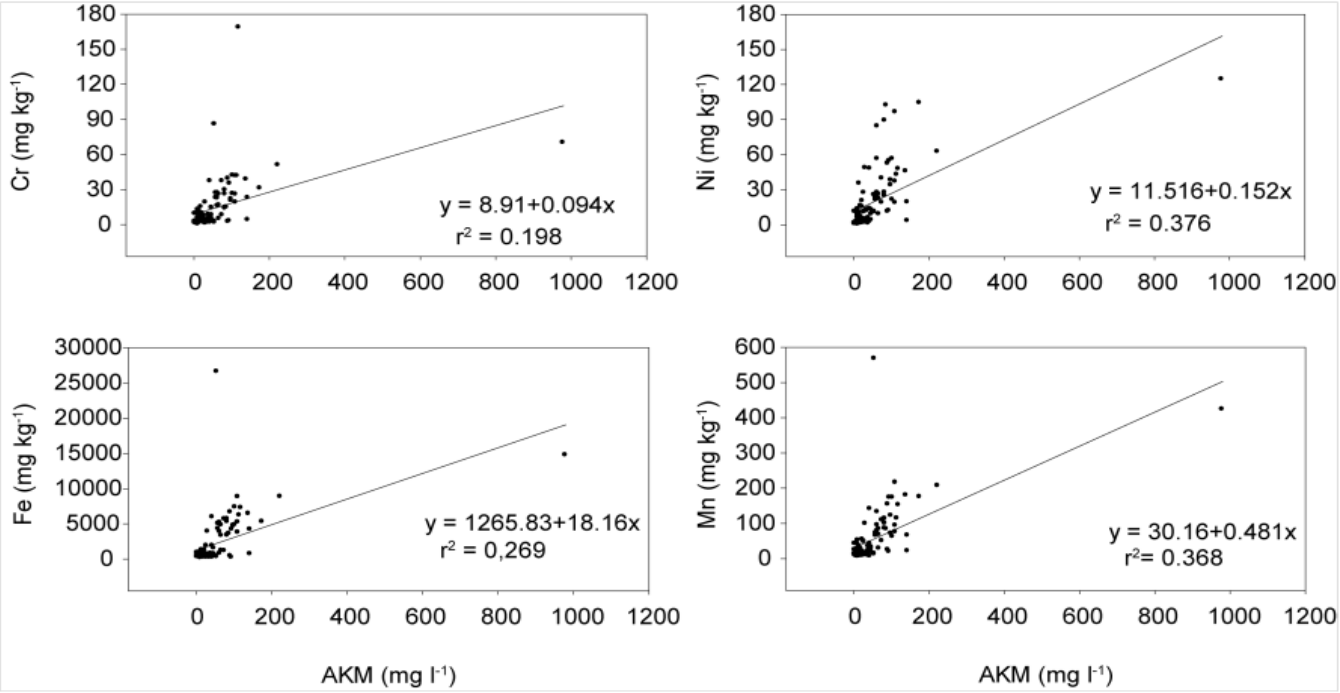

Figure 7. Correlation graphs between particulate Cr, Ni, Fe Mn and suspended solids.

pH and As, B and organic matter percentage with As, Ni, Zn elements. Annual means of dissolved trace elements were compared with WHO and EPA international standards. In lakes which have eutrophic status like Uluabat, trace elements absorbed to algae can pass to food web by release easily. Consequently, the lake will become more toxic when the probable decrease of pH. As a result, the long term monitoring and control of domestic and industrial wastewaters, restricted uses of agricultural pesticides are the important factors have to be taken into consideration in lake management. It is necessary to produce and apply new management strategies or plans in controlling point and non-point sources.

ACKNOWLEDGEMENTS

The project was funded by the Environment, Atmosphere, Earth and Marine Sciences group (ÇAYDAG- Project no: 107Y278) of the Scientific and Technical Research Council of Turkey (TÜBİTAK) and Scientific Research Foundation (Project no: M-2007/27) of Uludag University.

REFERENCES

Akdeniz S, Karaer F, Katip A, Aksoy E (2011). A GIS-based Method for Shallow Lake Eutrophication Assessment. J. Biol. Environ. Sci. 5(15):195-202.

Aksoy E, Özsoy G (2002). Investigation of multitemporal land use/cover and shoreline changes of the Uluabat Lake Ramsar site using RS and GIS, paper presented at the International Conference on Sustainable Land Use and Management, 13 October 2002, Turkey.

An Y, Kampbell DH (2003). Total, Dissolved, and Bioavailable Metals at Lake Texoma Marinas. Environ. Poll. 122:253-259.

Anonymous (2006a). *WHO,* A Compendium of Drinking-Water Quality Standards in The Eastern Mediterranean Region.

Anonymous (2006b). USEPA National Recommended Water Quality Criteria Correction Office of Water, EPA, 822-z-99-001, P. 25.

Anonymous (2007a). Terra/ Varian and Cem Brand ICP-MS/ICP-OES/AAS Microwave Digestion Seminar Notes, P. 81.

Anonymous (2007b). Minitab Inc. Meet Minitab, Release 15 for Windows, State College, PA.

APHA (1998). AWWA Standart Methods for the Examination of Water and Wastewater. American Public Heallth Association, 20th Edn. Washington, D. C.

Bailey MC, Hamilton DP (1997). Wind Induced Sediment Resuspension: a Lake-Wide Model. Ecol. Model. 99:217-228.

Bradl HB (2005). Heavy Metals in The Environment: Origin, Interaction and Remediation. Elsevier Academic Press. P. 269.

Burger J, Gochfeld M (2003). Heavy Metals in Commercial Fish in New Jersey. Environ. Res. 99:403-412.

Burton GA, Pitt RE (2002). Stormwater Effects Handbook, Lewıs Publıshers, CRC Press LLC. P. 929.

Che Y, He Q, Lin WQ (2003). The Distributions of Particulate Heavy Metals and Its Indication to The Transfer of Sediments in The Changjiang Estuary and Hangzhou Bay, China. Mar. Poll. Bull. 46:123-131.

Dalkıran N, Karacaoğlu D, Dere S, Sentürk E, Torunoğlu T (2006). Factors Affecting The Current Status of a Eutrophic Shallow Lake (Lake Uluabat, Turkey): Relationships Between Water Physical and Chemical Variables. Chem. Ecol. 22:279-298.

Fernández M, Cuesta S, Jıménez O, García MA, Hernández LM, Marina ML, González MJ (2000). Organochlorine and heavy metal residues in the water/sediment system of the Southeast Regional Park in Madrid, Spain. Chemosphere 41:801-812.

Filgueiras AV, Lavilla I, Bendicho C (2004). Evaluation of distribution, mobility and binding behaviour of heavy metals in surficial sediments of Louro River (Galicia, Spain) using chemometric analysis: A case

study. Sci. Total Environ. 330:115-129.
Gue´guen C, Dominik J (2003). Partitioning of Trace Metals Between Particulate, Colloidal and Truly Dissolved Fractions in a Polluted River: The Upper Vistula River (Poland). Appl. Geochem. 18:457-470.
İleri S (2010). The Assessment of physico-chemical parameters and geographic information system analysis of water and sediment quality of Lake Uluabat in terms of environment. MSc Thesis, Uludag University, Institute of Science, Bursa.
Ikem A, Egıebor NO, Nyavor K (2003). Trace Elements in Water, Fish and Sediment from Tuskegee Lake, Southeastern USA. Water, Air Soil Poll. 149:51-75.
Katip A (2010). Water quality monitoring of Lake Uluabat. PhD Thesis, Uludag University, Institute of Science, Bursa.
Katip A, Karaer F, Başkaya HS, İleri S, Sarmaşık S (2012a). Fraction distribution and risk assessment of heavy metals and trace elements in sediments of Lake Uluabat. Environ. Monit. Assess. 184:5399-5413.
Katip A, Karaer F, İleri S, Sarmaşık S, Aydoğan N, Zenginay S (2012b). Analysis and assessment of trace elements pollution in sediments of Lake Uluabat, Turkey. J. Environ. Biol. 33:961-968.
Nguyen HL, Leermakers M, Osán J, Török S, Baeyens W (2005). Heavy metals in LakeBalaton: Water Column, Suspended Matter, Sediment and Biota. Sci. Total Environ. 340:213-230.
Parsons RT, Strickland JD (1963). Discussion of Spectrofotometric Determination Of Marine Plant-Pigments With Revised Equations For As Certaining Chlorophyll and Corotenoids. J. Mar. Resour. 21:155-163.
Radojevic M, Bashkin, VN (1999). Practical Environmental Analysis., UK. Royal Soc. Chem. P. 466.
Shukla A, Zhang YH, Dubey P, Margrave JL, Shukla SS (2002). The role of sawdust in the removal of unwanted aterials from water. J. Hazard. Mater. B95:137-152.
Sigg L, Sturm M, Kistler D (1987). Vertical transport of heavy metals by settling particles in Lake Zurich. Limnol. Oceanogr. 32(l):112-130.
Straškraba M, Blažka P, Brandl Z, Hejzlar P, Komárková J, Kubečka J, Nesměrák I, Procházková L, Straškrabová V, Vyhnálek, V (1993). Framework for Investigation and Evaluation of Reservoir Water Quality in Czechosiovakia. Developments in Hydrobiology, Comp. Reservoir Limnol. Water Qual. Manage. 77:169-212.
Stumm W, Morgan J (1996). Aquatic Chemistry: An Introduction Emphasizing Chemical Equilibria in Natural Water, Wiley, New York, Third edn. pp. 655-666.
Yiğiterhan O, Murray JW (2008). Trace Metal Composition of Particulate Matter of The Danube River and Turkish Rivers Draining into The Black Sea. Mar. Chem. 111:63-76.

UPCOMING CONFERENCES

ICNMB 2013 : International Conference on Nuclear Medicine and Biology Switzerland, Zurich, July 30-31, 2013

International Conference on Mathematical Modeling in Physical Sciences Prague, Czech Republic, September 1-5, 2013

Conferences and Advert

July 2013
ICNMB 2013 : International Conference on Nuclear Medicine and Biology
Switzerland, Zurich, July 30-31, 2013

September 2013
International Conference on Mathematical Modeling in Physical Sciences
Prague, Czech Republic, September 1-5, 2013

International Journal of Physical Sciences

Related Journals Published by Academic Journals

- *African Journal of Pure and Applied Chemistry*
- *Journal of Internet and Information Systems*
- *Journal of Geology and Mining Research*
- *Journal of Oceanography and Marine Science*
- *Journal of Environmental Chemistry and Ecotoxicology*
- *Journal of Petroleum Technology and Alternative Fuels*

academicJournals